Brodogradnja Volume 75, Number 3 (2024) 75304

journal homepage: www.brodogradnja.fsb.hr

Brodogradnja

An International Journal of Naval Architecture and Ocean Engineering for Research and Development

Application of an offline grey box method for predicting the manoeuvring performance

Elis Atasayan[1,2], *Evgeni Milanov*[3], *Ahmet Dursun Alkan*[2*]

[1] *Department of Naval Architecture and Marine Engineering, Turkish Naval Academy, National Defence University, Türkiye*
[2] *Department of Naval Architecture and Marine Engineering, Naval Architecture and Maritime Faculty, Yildiz Technical University, Türkiye*
[3] *BSHC-Bulgarian Ship Hydrodynamics Centre - IMSETHC, Bulgarian Academy of Sciences, Bulgaria*

ARTICLE INFO

Editor-in-Chief: Prof. Nastia Degiuli
Associate Editor: PhD Ivana Martić

Keywords:
System identification
Ship manoeuvring performance
Grey box method

ABSTRACT

The prediction of manoeuvring performance for safe navigation and effective design of ships increasingly depends on artificial intelligence (AI), mainly digital twin technology. This technology requires a digital model of the physical ship. The hydrodynamic coefficients and parameters of these models are commonly obtained through two experimental methods: the planar motion mechanism (PMM) and the circular motion test (CMT). These methods are time-consuming and expensive, which may not be feasible during the early stages of the design process. This study investigates a cost-effective alternative approach to these methods by implementing a grey box method on ships. For the first of these implementations, a full-scale tanker ship was applied with artificial training data of zigzag manoeuvres. A validation study was carried out by comparing the simulation and free-running model test results of the tanker. For the second of these implementations, a scale model of a car carrier was selected, and several numerical search methods were combined to obtain a more accurate digital model. The 3-degree-of-freedom (DOF) Manoeuvring Modelling Group (MMG) models identified through this combination were validated with simulations and compared with the free-running model test results for various manoeuvres. The contribution of this study lies in the accurate capture of the manoeuvring characteristics of the physical model, which is achieved through the use of the adjustment interval and the combination of various numerical search method of the grey box method. Consequently, the developed model can be used in future studies as a faster decision-making tool for determining the straight-line stability or instability of a ship in the ship design and in predicting the manoeuvring performance of the ship.

1. Introduction

The growing global adoption of electric vehicles is aimed at reducing the carbon footprint of passenger vehicles, thereby increasing the importance of car carriers in transporting these vehicles to ports [1]. The use of new technologies such as digital twins on surface ships has the potential to help stop the rising global

* Corresponding author.
E-mail address: alkanad@yildiz.edu.tr

http://dx.doi.org/10.21278/brod75304
Submitted 04 March 2024; Accepted 12 May 2024
ISSN 0007-215X; eISSN 1845-5859

warming threat by reducing CO2 emissions and to increase maritime safety by preventing possible ship collisions in marine environments [2]. As vehicle carriers are also expected to become autonomous as a result of digitalisation, in this study emphasises the importance of predicting and simulating the manoeuvring characteristics of car carriers with a digital model in order to meet the increasing demands of marine transportation.

Various methods are used to predict surface ship manoeuvrability, including database and model testing [3] methods such as empirical formulas [4], full-scale trials [5], free-running model tests [6], System Identification (SI) [6], captive model tests like Planar Motion Mechanism (PMM) [7], and Circular Motion Test (CMT) [8], as well as virtual captive model tests (VCMT) [9] . Each method offers unique insights. Firstly, empirical methods, which are based on model scale experiments or full-scale sea trials, are typically employed at the preliminary design stage. Although empirical methods provide preliminary information about the ship's manoeuvring and course-keeping ability, their sensitivity is low. The use of such formulas carries the risk of erroneous results when the data limits are exceeded [10]. It is necessary to supply the hydrodynamic forces and derivatives from the captive model test when the limits are far from those of the database [3]. Secondly, full-scale trials represent a valuable source of real-world data for the assessment of whether a ship complies with the International Maritime Organization (IMO)'s recommended manoeuvring characteristics at the final stage of the design cycle. The advantage of full-scale trials is that the scale effect between the full-scale ship and its scale model can be avoided [11]. Nevertheless, test environments with wind, waves, and currents where calm water conditions cannot be achieved during full-scale sea trials present a challenge, as they require more processing of measurement data, such as trajectory correction, compared to scale model tests carried out in the manoeuvring basin [12]. Thirdly, free-running test results can provide directly assess inherent directional stability [13] and manoeuvring performance, only requiring a large enough basin or lake to carry out manoeuvres in good weather conditions, such as calm water. However, they do not provide data on the effects of hull and appendages separately. First of the captive methods, PMM can determine the complete set of hydrodynamic coefficients of a ship moving through a fluid [13]. It also provides essential data related to the effects of the hull and appendages separately. Also, the other captive method of CMT reduces uncertainties regarding hydrodynamic forces and moments because it has zero motion frequency [14]. Despite the advantages of captive tests, they are expensive [13] and require a quite wide towing tank in order to prevent boundary effects from the walls of the towing tank [15]. Final method, system identification, is the process of deriving the parameters of the ship motion equations describing a ship's characteristics through the application of mathematical optimization [16]. In contrast to a large number of captive model tests, the SI method provides an opportunity for the estimation of all coefficients and parameters with the use of a single or a few free-running tests [17]. While identification can be achieved through model-scale free-running tests, SI can also be accomplished with full-scale sea trials and simulation data [18]. SI methods can be economical alternatives for determining hydrodynamic coefficients and parameters compared to captive tests [19]. However, this approach also has disadvantages. Although mathematical model with the determined coefficients and parameters can accurately predict the ship's manoeuvrability, as evidenced by the experimental test results, there is a possibility that the determined coefficients and parameters may differ from the actual values [16]. Following a comprehensive evaluation of the available methods, it can be concluded that the SI method represents the superior alternative to other methods in terms of its highly effective, useful, and cost-effective approach for determining coefficients and parameters.

SI methods range from simple determinations to complex algorithms [20] and can be divided into three categories [21,22]. The initial method, white-box modelling, also called parametric models [23], usually refers to a mathematical model [24] and is completely based on physical laws. Furthermore, white box modelling can eliminate the scale effect and improve the accuracy of the prediction appropriately [22]. However, despite these advantages, white box modelling may be subject to excessive computation in the calculation of coefficient values [24]. A further category, black box models, also called non-parametric models [23], can be flexible and easy to implement, but on the other hand, they are completely data-driven and have poor generalisation properties due to their lack of physical meaning [22]. Grey box modelling lies between white box modelling and black box modelling and grey box modelling takes the strengths of both models and avoids their disadvantages. Moreover, grey box modelling can be used in the creation of digital twin based models for the control and prediction of ship motion [21]. Also, in grey box modelling, a mathematical model

representing the known part of the system is established to ensure rapid generalisability [22]. In light of these evaluations, the present study seeks to investigate the application of grey box modelling through the use of appropriate mathematical models.

Various conventional mathematical models are available to represent ship manoeuvrability. These models are commonly used by naval architects, ship designers, and ship operators to improve ship designs and enhance ship handling and safety. Nomoto et al. [25] developed linear [26] and nonlinear models. The linear model is widely used in ship autopilots due to its simplicity. However, it is only valid for small yaw rates and sway velocities because of its linearity. Additionally, there are two other commonly used methods for consideration: the Abkowitz model developed by Abkowitz [26] and the MMG model proposed by Ogawa and Kasai [27] and later described by Yoshimura [28], Yasukawa and Yoshimura [14]. The Abkowitz model considers the hull, rudder, and propeller as a single rigid body, whereas the MMG Model divides them into separate components, including the hull, propeller, and rudder [28]. The primary challenge in the Abkowitz and MMG mathematical manoeuvring models has been estimating hydrodynamic coefficients, also known as manoeuvring derivatives, accurately. To overcome this difficulty, variety of grey box SI methods have been proposed as alternatives to aforementioned captive model tests.

Notable various methods from grey box modelling among SI methods are presented in this part of the study. In the study of Milanov [29], the author successfully applied the offline grey box method, precisely the Trust Region Reflective Newton Optimization (TRR) method, which is one of the SI methods, to KRISO Container Ship (KCS), a benchmark ship. In another study of Efremov and Milanov [30], the authors also applied the same TRR method to a surface vessel equipped with twin propellers and rudders. On these two studies, the ship dynamics were identified for determining Abkowitz's mathematical model coefficients and validated with turning manoeuvre data. These studies also demonstrated the effectiveness of the TRR method in capturing and simulating the 3-DOF ship dynamics. It is important to highlight that Milanov [29] and Efremov and Milanov [30] accessed the initial coefficients in TRR through PMM test. The study of Liu et al. [31] presented an overview of the identification process. They compared the capabilities and challenges of offline grey and black box methods for determining the coefficients of Abkowitz's mathematical model of the the second variant of the MOERI tanker KRISO Very Large Crude Carrier (KVLCC2) using zigzag maneuver data. Zhang et al. [32] implemented the target-oriented crow search algorithm for determining the second-order linear and nonlinear Nomoto model coefficients of fast ferry. Their study demonstrated a precise offline method for accessing a ship's heading angle and yaw rate data, which is beneficial for autonomous navigation control systems of ships and for determining the Nomoto model coefficients with less data. However, their study is limited to control applications. Alexandersson et al. [33] used advanced offline methods, such as the Extended Kalman Filter (EKF) with a Rauch Tung Striebel (RTS), to obtain the coefficients of linear, Abkowitz, and modified Abkowitz mathematical models for a twin-screw wind-powered car carrier (wPCC) with good stability and symmetrical hydrodynamic manoeuvring forces. Chen et al. [34] presented an offline grey-box model based on the 4-DOF MMG model, utilizing the least square support vector machine (LS-SVM) method by implementing different levels of noise to the training datasets of SR108 container ship for parameter identification, and demonstrated the model's robustness under disturbance. In order to generate the artificial training datasets, the researchers conducted simulations of zigzag manoeuvres with rudder angles ranging from $\pm 10^\circ$ to $\pm 30^\circ$. Zhang et al. [35] explored online grey-box modelling with SVM to Abkowitz mathematical model for capturing 3-DOF ship manoeuvring motion of the Mariner ship model, compared online and offline SVM, and demonstrated that the performance of their proposed online SVM on the data of $+20^\circ / -20^\circ$ zigzag manoeuvre was preferrable to the offline SVM. Chillcce and Moctar [36] applied an offline LS method to identify the coefficients of the 3-DOF Abkowitz mathematical model of the KVLCC2 tanker. The training data used in their study were obtained from numerical simulations, which differed from the measurement data often subject to noise. The simulations included a $+10^\circ / -10^\circ$ zigzag manoeuvre and were validated with $+35^\circ / -35^\circ$ zigzag manoeuvre and $+35^\circ$ turning circle test. Chillcce and Moctar [36] obtained the initial coefficients for fine-tuning through the literature. In their study, they applied the lower and upper bounds on the hydrodynamic derivatives that varied between -1.00 and $+1.00$ in their study. Sutulo and Guedes Soares [37] presented an offline genetic algorithm (GA) method to identify the artificial virtual ship's

parameters of a 3-DOF mathematical model using artificial training data of a $+30°/-30°$ zigzag manoeuvre. In their research, the upper and lower bounds of the mathematical model were extended to different ranges, starting from -1.00 to $+1.00$ and extending from -10.00 to $+50.00$. Their study demonstrated that the implementing extremely large ranges resulted in a significant search difficulty. Moreover, they emphasised that the spiral test is paramount importance in evaluating the efficacy of mathematical models. Han et al. [22] proposed an offline grey-box model based on the 3-DOF Abkowitz model. Furthermore, they employed a data-driven model for hydrodynamic correction terms developed with a feedforward neural network using data from free-running model tests. Their findings demonstrated enhanced prediction accuracy. Jiang et al. [24] presented a multi-objective optimal input design method aimed at improving both the accuracy and robustness of model and accuracy and identifying the offline grey-box model based on 4-DOF MMG mathematical model for SR108 container ship, and incorporating the correlation factor to minimize the parameter drift. Their findings demonstrated the superiority and efficacy of the proposed method in terms of generalizability.

According to the authors of this study, considering the cited publications on predicting ship manoeuvrability based on grey box modelling, more comprehensive studies are needed to examine ship manoeuvring characteristics by determining the parameters of the 3-DOF MMG model for a single-screw ship, which is a car carrier that exhibits dynamic instability. The authors of this study highlight that the TRR method is not combined with free-running test data in parameter estimation of car carriers as a significant shortcoming. Another point to consider is that research on car carriers has not adequately focused on capturing and assessing course-keeping ability using the pull-out manoeuvre and spiral tests. This spiral test was emphasized in the study of Sutulo and Guedes Soares [37] as being of great importance in evaluating the effectiveness of mathematical models. In order to compensate for these gaps, the TRR grey box modelling of the SI method was applied to identify the parameters of the 3-DOF MMG mathematical model, which differs from the mathematical models used by Milanov [29], and Efremov and Milanov [30], for car carrier in this study.

This study implemented a $+20°/-20°$ zigzag manoeuvre on the car carrier model using the grey box model and verified it with turning circle tests using $+35°$ starboard and $-35°$ port rudder angle, pull-out tests, and spiral tests. The study differs from Milanov [29] and Chillcce and Moctar [36] in terms of the verification data used. Unlike Milanov [29] and Chillcce and Moctar [36], who obtained the initial coefficients through PMM tests and literature, this study empirically estimated initial coefficients. The identification procedure is similar to that used by Milanov [29], and Efremov and Milanov [30], but combining search methods with TRR differs from those used in previous studies. In addition to the combined search method, the authors of this study focus more on obtaining a physically realistic solution, for which they applied constraints varied between -8.00 and $+1.50$ on the hydrodynamic coefficients and parameters, specifically for the car carrier. The validation of this grey box model is carried on by predicting the zigzag manoeuvre of the KVLCC2 tanker with data on a rudder angle of $-20°/+20°$ obtained from the open-source MANSIM tool [38]. The identified model was used to simulate the manoeuvre, and the results were compared to the literature provided for model scale in [39] and plotted for full scale in [38].

The paper is structured as follows: Section 2 describes the digital model of physical ship, and Section 3 describes the system identification algorithm of the digital model separately. Section 4 presents numerical results and discusses them. Section 5 describes practical implications and future directions, while Section 6 concludes the paper.

2. Ship mathematical model

The mathematical model developed by Yoshimura [28], Yoshimura and Masumoto [40], and Yasukawa and Yoshimura [14] can be used to predict and simulate the manoeuvring motions of a single propeller and single rudder ship in calm water. The following subsections explain further details, including the ship motion coordinate system, variable non-dimensionalization, and equations for hydrodynamic forces and moments acting on the hull, propeller, and rudder.

2.1 Coordinate systems and non-dimensionalization

The motion of a ship during manoeuvring involves two coordinate systems: space-fixed (o_0 - $x_0y_0z_0$) and ship-fixed (o - xyz). Both coordinate systems were used in this study, as described in detail by Yasukawa and Yoshimura [14] and shown in Fig. 1. The x_0 - y_0 plane of the space-fixed coordinate system was aligned with the calm water surface, and the z_0 axis was oriented vertically downward. The ship-fixed coordinate system o - xyz was defined by the origin o located at the midship of the ship with the x -axis oriented towards the bow of the ship, the y -axis towards the starboard side of the ship, and the z -axis downward of the ship. The velocity components in the ship-fixed coordinate system can be transformed to the space-fixed coordinate system using the equations $u_0 = (u\cos\psi - v\sin\psi)$ and $v_0 = (u\sin\psi + v\cos\psi)$ where ψ is the heading angle between the x_0 and x axis.

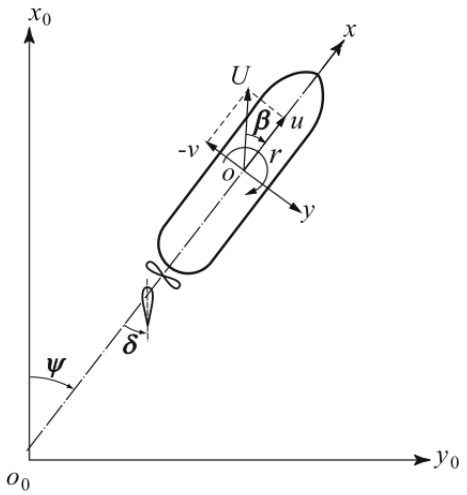

Fig. 1 Earth-fixed and ship-fixed coordinate systems [14]

In this study, hydrodynamic forces and moment acting on the hull, propeller, and rudder, as well as the mass, added mass, moment of inertia, and added moment of inertia, are non-dimensionalized, as expressed in the study by Sukas et al. [38]. The prime symbol (') next to the parameters of motion equations indicates their non-dimensionalization. The hydrodynamic forces X and Y are non-dimensionalized by $(1/2)\rho U^2 Ld$, while moment N is non-dimensionalized by $(1/2)\rho U^2 L^2 d$. The velocity components surge, u, sway, v, yaw rate, r, are non-dimensionalized for u, and v by U and for r by U/L. Additionally, the mass and added mass are non-dimensionalized by $(1/2)\rho L^2 d$, while the yaw moment of inertia and added yaw moment of inertia are non-dimensionalized by $(1/2)\rho L^4 d$. The variables used are U for the total speed of the ship, ρ for the water density, L for the length between perpendiculars, and d for the ship's draught.

2.2 Motion equations of the dynamic model

The 3-DOF MMG model, known for incorporating nonlinear aspects and capturing hydrodynamic interactions in ship manoeuvring, is employed in this study by utilizing Eq. (1), which includes the hydrodynamic surge force of X and sway force of Y, and the yaw moment of N, as presented in the study of Sukas et al. [38]. Due to the calm water test conditions, heave, pitch, and roll motions are neglected. Simulation studies by Wu et al. [41] support the validity of this 3-DOF MMG model by adding wind and wave terms, which can be used to prevent collisions between multiple autonomous surface vehicles in wind and wave conditions.

$$\begin{aligned}(m+m_x)\dot{u}-(m+m_y)vr-x_G mr^2 &= X\\ (m+m_y)\dot{v}-(m+m_x)ur-x_G m\dot{r} &= Y\\ (I_{zG}+x_G^2 m+J_z)\dot{r}+x_G m(\dot{v}+ur) &= N\end{aligned} \tag{1}$$

Here, I_{zG} represents the yaw moment of inertia and is assumed to be approximately $m(0.25L)^2$ for typical merchant ships. The dot notation $(\dot{.})$ indicates the time-dependent derivatives of the relevant parameters. In Eq. (1), x_G represents the longitudinal coordinate of the ship's center of gravity, as given in Table 1, where m represents the mass of the ship, while m_x and m_y represent the added masses resulting from the ship's motion in the x and y-directions, respectively. The empirical formulas given in Eq. (2) presented in the study by Sukas et al. [38] were used to calculate the added mass values of m_x and m_y and their value of the coefficients are presented in Table A.1 for the car carrier. In Eqs. (2) and (3) use the main particulars of the ship, which are described in Table 1 as L, B, d, and C_B.

$$\begin{aligned}m_x &= m(0.05)\\ m_y &= m\left[\begin{array}{l}\left(0.882-0.54C_B(1-1.6\frac{d}{B}\right)-0.156\left(1-0.673C_B\right)\frac{L}{B}\\ +0.826\frac{d}{B}\frac{L}{B}\left(1-0.678\frac{d}{B}\right)-0.638C_B\frac{d}{B}\frac{L}{B}\left(1-0.669\frac{d}{B}\right)\end{array}\right]\end{aligned} \tag{2}$$

In Eq. (1), J_Z defines the added yaw moment of inertia, and the value of the coefficient is calculated for the car carrier using the empirical formula in Eq. (3) taken from Sukas et al.'s [38] study and presented in Table A.1.

$$J_z = m\left[\frac{1}{100}(33-76.85C_B(1-0.784C_B)+3.43\frac{L}{B}(1-0.63C_B))\right]^2 \tag{3}$$

The 3-DOF motion in Eq. (1) can be expressed in matrix form as follows:

$$\begin{bmatrix}m+m_x & 0 & 0\\ 0 & m+m_y & x_G m\\ 0 & x_G m & I_{zG}+x_G{}^2 m+J_z\end{bmatrix}\begin{bmatrix}\dot{u}\\ \dot{v}\\ \dot{r}\end{bmatrix}+\begin{bmatrix}0 & 0 & 0\\ 0 & 0 & (m+m_x)u\\ 0 & 0 & x_G mu\end{bmatrix}\begin{bmatrix}u\\ v\\ r\end{bmatrix}=\begin{bmatrix}X\\ Y\\ N\end{bmatrix} \tag{4}$$

The first term of the right-side of Eq. (4) represents the mass matrix M. Eq. (4) is rearranged so that the acceleration matrix is remained on the left-hand side, as shown in Eq. (5).

$$\begin{bmatrix}\dot{u}\\ \dot{v}\\ \dot{r}\end{bmatrix}=\begin{bmatrix}\frac{1}{M_{11}} & 0 & 0\\ 0 & \frac{M_{33}}{\det M} & \frac{-M_{32}}{\det M}\\ 0 & \frac{-M_{23}}{\det M} & \frac{M_{22}}{\det M}\end{bmatrix}\begin{bmatrix}X+(m+m_y)vr+rx_G mr\\ Y-(m+m_x)ur\\ N-x_G mur\end{bmatrix} \tag{5}$$

The determinant of matrix M, denoted by $\det M$, is explained in Eq. (6) as:

$$\det M = M_{22}M_{33}-M_{23}M_{32} \tag{6}$$

The values of M_{11}, M_{22}, M_{23}, M_{32}, and M_{33} are calculated by the following formulas: $(m+m_x)$, $(m+m_y)$, $(x_G m)$, and $(I_{zG}+x_G{}^2 m+J_z)$, respectively.

X, Y, and N, stated in Eq. (1) can be subdivided due to MMG's modular structure as follows:

$$\begin{aligned} X &= X_H + X_P + X_R \\ Y &= Y_H + Y_R \\ N &= N_H + N_R \end{aligned} \tag{7}$$

The MMG mathematical model considers hydrodynamic forces and moments in a modular way, as shown in Eq. (7). The forces and moments given on the right-hand side of Eq. (7) are denoted by the subscripts H, P, and R representing the contributions of the hull, propeller, and rudder, respectively as stated in [38]. In this model, it is assumed that the propeller only provides forward thrust on the x-axis, in which case, Y_P and N_P are zero.

The sub-sections following Eq. (7) explain the different methods used to obtain each hydrodynamic force and moments in the second matrix on the right-hand side.

2.2.1 Hull forces and moment

The forces acting on the hull, X_H, and Y_H, and the moment N_H, are expressed as the first and third-order polynomial functions of sway velocity v and yaw rate r are as follows [38]:

$$\begin{aligned} X_H &= -X_0 + X_{vv}v^2 + X_{vr}vr + X_{rr}r^2 + X_{vvvv}v^4 \\ Y_H &= Y_v + Y_r r + Y_{vvv}v^3 + Y_{vvr}v^2 r + Y_{vrr}vr^2 + Y_{rrr}r^3 \\ N_H &= N_v + N_r r + N_{vvv}v^3 + N_{vvr}v^2 r + N_{vrr}vr^2 + N_{rrr}r^3 \end{aligned} \tag{8}$$

Here, X_0 is the resistance coefficient. Its value is calculated using the Holtrop Mennen method [42,43] to reliably estimate resistance in the early stages of ship design, as stated in Xhaferaj's study [44].

To obtain the hydrodynamic derivatives described in Eq. (8), captive model tests and the VCMT can be employed as an entry for the mathematical model [33]. However, as these methods are costly, they were not used in this study. In addition to the aforementioned methods, free-running and full-scale tests can also be used as inputs for the manoeuvring model. However, these two methods do not directly yield the aforementioned derivatives. As this study aims to identify these derivatives from free-running test data using the grey box method, which is a system identification method, it is necessary to provide estimated values for these derivative values at the beginning of the estimation process. Empirical formulas stated in Eqs. (9) and (10) were used in the present study to expedite the acquisition of the required values. To estimate the linear coefficient of hydrodynamic sway force acting on the hull Y_H and the yaw moment N_H, empirical formulas can be expressed as follows [38]:

$$\begin{aligned} Y_v &= \left[-\pi \left(\frac{d}{L} \right)^2 \left(1 + \frac{1.4}{\pi} C_B \frac{B}{d} \right) \right] \frac{L}{d} \\ Y_r &= \left[-0.5 \left(-\pi \left(\frac{d}{L} \right)^2 \right) \right] \frac{L}{d} \\ N_v &= \left[\left(-\pi \left(\frac{d}{L} \right)^2 \frac{2}{\pi} \right) \right] \frac{L}{d} \\ N_r &= \left[-\pi \left(\frac{d}{L} \right)^2 \left(\frac{1.04}{\pi} - \frac{4}{\pi} \frac{d}{L} \right) \right] \frac{L}{d} \end{aligned} \tag{9}$$

The empirical formulae for estimating the nonlinear coefficient of the hydrodynamic surge and sway forces acting on the hull X_H , Y_H , and the yaw moment N_H can be expressed as follows [38]:

$$
\begin{aligned}
X_{vv} &= \left(1.15\frac{C_B}{L/B}\right) - 0.18 \\
X_{vr} &= \left(m_y - 1.91\frac{C_B}{L/B}\right) + 0.08 \\
X_{rr} &= \left(-0.085\frac{C_B}{L/B}\right) + 0.008 - x_G m_y \\
X_{vvvv} &= \left(-6.68\frac{C_B}{L/B}\right) + 1.10 \\
Y_{vvv} &= -\left(0.185\frac{L}{B} + 0.48\right) \\
Y_{vvr} &= -0.75 \\
Y_{vrr} &= -\left(0.26\left(1 - C_B\right)\frac{L}{B} + 0.11\right) \\
Y_{rrr} &= -0.051 \\
N_{vvv} &= -\left[-0.69C_B + 0.66\right] \\
N_{vvr} &= \left[\left(\frac{1.55C_B}{L/B}\right) - 0.76\right] \\
N_{vrr} &= \left[-0.075\left(1 - C_B\right)\frac{L}{B} - 0.098\right] \\
N_{rrr} &= \left[\left(\frac{0.25C_B}{L/B}\right) - 0.056\right]
\end{aligned}
\tag{10}
$$

Table A.1 in Appendix 1 presents the estimated linear and non-linear coefficients of the car carrier calculated using the empirical formulae mentioned above.

2.2.2 Propeller and rudder forces and moment

The force due to the propeller in the *x*-axis of X_P is expressed as follows:

$$X_P = \left(1 - t_P\right)T_P \tag{11}$$

Here, t_P represents the propeller thrust reduction coefficient and is considered to be 0.2700 for the car carrier as stated in Sukas et al.'s [38] study. T_P represents the thrust propeller and is calculated using the empirical formula shown in Eq. (12) as given [38].

$$T_P = \rho n^2 D_P^4 K_T \tag{12}$$

Here, the thrust coefficient K_T is presented as a second-order polynomial function of the propeller advance ratio, J_P. K_T can be calculated as follows:

$$K_T = k_0 + k_1 J_P + k_2 {J_P}^2 \tag{13}$$

The propeller model used in this study for the car carrier is within the specified ranges, namely blade numbers Z ranging from 2 to 7, blade area ratios A_E/A_0 ranging from 0.30 to 1.05, and pitch ratios P/D_P ranging from 0.5 to 1.4, to evaluate the K_T for Wageningen B-series propeller models. The coefficients k_0, k_1, and k_2 for expressing K_T for the car carrier were estimated as 0.4084, -0.2917, and -0.1211 from the propeller series above mentioned according to the polynomials given in the study of Oosterveld and Van Oossanen [34]. Where J_P can be calculated as follows:

$$J_P = \frac{u_P}{nD_P} \tag{14}$$

Here, u_P represents inflow velocity to propeller as follows:

$$u_P = u\left(1 - w_P\right) \tag{15}$$

where w_P is the wake coefficient of the propeller. The wake coefficient w_P, which varies during the manoeuvre, is given as follows [38]:

$$w_P = w_{P0}\exp\left(-4\beta_P{}^2\right) \tag{16}$$

Here, w_{P0} is the effective wake fraction, which can be estimated, using the empirical formula as stated in the study by Sukas et al. [38].

$$w_{P0} = 0.5C_B - 0.05 \tag{17}$$

where β_P is the geometrical inflow angle to the propeller as stated in the study by Dai et al. [9], and can be calculated as follows:

$$\beta_P = \beta - \frac{x_P}{L}r' \tag{18}$$

Here β represents the drift angle of the ship and can be calculated by the formula $\tan^{-1}(-v/u)$ as stated in the study by Dai et al. [9], while x_P represents the distance of the propeller from the midship.

The modelling of the hydrodynamic surge force X_R on the x-axis, sway force Y_R on the y-axis, and the yaw moment N_R on the z-axis induced by the rudder are calculated using the following equations [38]:

$$\begin{aligned} X_R &= -\left(1 - t_R\right)F_N \sin\delta \\ Y_R &= -\left(1 + a_H\right)F_N \cos\delta \\ N_R &= -\left(x_R + a_H x_H'\right)F_N \cos\delta \end{aligned} \tag{19}$$

Here, t_R, a_H, and x_H' are the hull-rudder interaction parameters, and can be calculated using empirical formulae as presented in the study by Sukas et al. [38]:

$$\begin{aligned} t_R &= 0.39 \\ a_H &= 3.6C_B\frac{B}{L} \\ x_H' &= -0.40 \end{aligned} \tag{20}$$

For the car carrier, x_R is the longitudinal coordinate of the rudder position, and can be approximated as $-L/2$ as presented in the study by Yoshimura and Masumoto [40]. Where F_N represents the rudder normal force as defined by Sukas et al. [38] and is as follows:

$$F_N = 0.5\rho A_R {U_R}^2 f_\alpha \sin\alpha_R \tag{21}$$

Here A_R represents the rudder profile area, and f_α represents the rudder lift gradient coefficient and can be calculated as presented by Sukas et al. [38]:

$$f_\alpha = \frac{6.13\Lambda}{\Lambda + 2.25} \tag{22}$$

where Λ represents the rudder aspect ratio, U_R represents the inflow velocity to the rudder and is calculated as follows [38]:

$$U_R = \sqrt{{u_R}^2 + {v_R}^2} \tag{23}$$

where α_R is effective inflow angle to the rudder and is as follows [38]:

$$\alpha_R = \delta - \tan^{-1}\left(v_R/u_R\right) \tag{24}$$

Here, u_R and v_R are components of the inflow velocity to rudder. The lateral component v_R can be calculated as follows [38]:

$$v_R = \gamma_R \beta_R \tag{25}$$

where γ_R is the flow-straightening coefficient of sway velocity for the rudder. The upper and lower values for the γ_R coefficient are as follows [38]:

$$\begin{aligned}
\gamma_{R_{upper}} &= 23.708 - 83.84C_B + 173.72\left(\frac{2d}{L}\right) + 71.64C_B^2 + 157\left(\frac{2d}{L}\right)^2 - 261.11C_B\left(\frac{2d}{L}\right) \\
\gamma_{R_{lower}} &= 6.8736 - 16.77C_B + 3.5687\left(\frac{2d}{L}\right) + 4.68C_B^2 - 253.14\left(\frac{2d}{L}\right)^2 + 74.83C_B\left(\frac{2d}{L}\right)
\end{aligned} \tag{26}$$

where β_R represents the effective inflow angle to the rudder in manoeuvring and is as follows:

$$\beta_R = \beta - l_R' r' \tag{27}$$

Here, l_R' is the flow-straightening coefficient of the yaw rate for the rudder and can be calculated as follows [38]:

$$l_R' = 1.7C_B\frac{B}{L} - 1.2 \tag{28}$$

The longitudinal component u_R can be calculated as follows [38]:

$$u_R = \varepsilon u_P\left(1 - w_P\right)\sqrt{\eta\left\{1 + \kappa\left(\sqrt{1 + \frac{8K_T}{\pi {J_P}^2}} - 1\right)\right\}^2 + \left(1 - \eta\right)} \tag{29}$$

Here ε is the ratio of the effective wake fraction in the way of the propeller and rudder and can be calculated as follows [38]:

$$\varepsilon = 2.26 - 1.82\left(1 - w_{P0}\right) \tag{30}$$

where η represents the ratio of propeller diameter to rudder span. κ is an experimental constant for expressing longitudinal component u_R and κ can be calculated by the following formula [38]:

$$\kappa = \frac{0.55}{\left[2.26 - 1.82\left(1 - w_{P0}\right)\right]} \tag{31}$$

3. System identification method

The fundamental principle of the SI process is to fit the coefficients and parameters of a mathematical model to observed input and output data through optimization, as shown in Fig. 2. The process of SI requires inputting a signal $\underline{u}(t)$ into the system and observing the output $\underline{y}(t)$. The input $\underline{u}$ of the process is the measured rudder angle of the ship (δ), while the outputs are the measured velocity components of the ship (u, v, and r), which constantly change depending on time. Then, the predicted response of the digital model $\underline{\hat{y}}(t)$ at each time step is then compared with the actual system output.

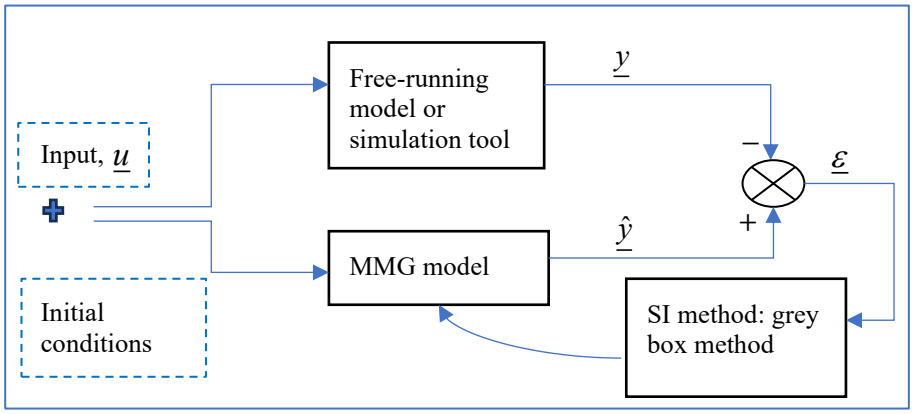

Fig. 2 Diagram of the system identification process for ship manoeuvring

3.1 State-space representation of grey box model

To initiate the SI process, it is necessary to construct a continuous-time state space representation, which is a mathematical model of a physical system [45]. The general form of a state-space model can be expressed as follows:

$$\begin{aligned}
&\dot{\underline{x}}(t) = f\left(t, \underline{x}(t), \underline{u}(t), \theta\right) \\
&\underline{y}(t) = h\left(t, \underline{x}(t), \theta\right) \\
&\underline{x}(0) = \underline{x}^0 \\
&\theta = \begin{bmatrix} -X_0' & X_{vv}' & X_{vr}' & X_{rr}' & X_{vvvv}' & Y_v' & Y_r' & Y_{vvv}' & Y_{vvr}' & Y_{vrr}' & Y_{rrr}' & N_v' & N_r' & N_{vvv}' & N_{vvr}' & N_{vrr}' & N_{rrr}' & l_r' \\ \varepsilon & m_x' & m_y' & J_z' & t_R & a_H & x_H' & t_P & w_{P0} & \gamma_{R_{upper}} & \gamma_{R_{lower}} & & & & & & & \end{bmatrix}^{\mathrm{T}}
\end{aligned} \tag{32}$$

Here, θ is the parameter vector to be identified during the SI process, and $\underline{x}(0)$ is the value of the initial state used by the solver at the starting point. The first equation, $\dot{\underline{x}}(t)$, represents the state equation of the digital model, while the second equation, $\underline{y}(t)$, represents the observation (output) equation. $\underline{u}(t)$ is the input vector and equal to the rudder command, δ. The state equations of the 3-DOF MMG model are as follows in more detail,

$$\begin{aligned}
\underline{\dot{x}}_1(t) &= \dot{u} = \frac{X + \left(m + m_y\right)vr + x_G mr^2}{M_{11}} \\
\underline{\dot{x}}_2(t) &= \dot{v} = \frac{-\left(-M_{33}\left(Y - \left(m + m_x\right)ur\right) + M_{32}\left(N - x_G mur\right)\right)}{\det M} \\
\underline{\dot{x}}_3(t) &= \dot{r} = \frac{\left(-M_{23}\left(Y - \left(m + m_x\right)ur\right) + M_{22}\left(N - x_G mur\right)\right)}{\det M}
\end{aligned} \tag{33}$$

Selecting state variables $\underline{x}_1(t) = u$, $\underline{x}_2(t) = v$, and $\underline{x}_3(t) = r$, the observation equations of 3-DOF MMG can be written as follows:

$$\begin{aligned}
\underline{y}_1(t) &= \underline{x}_1(t) \\
\underline{y}_2(t) &= \underline{x}_2(t) \\
\underline{y}_3(t) &= \underline{x}_3(t)
\end{aligned} \tag{34}$$

3.2 Optimization methods

The coefficients and parameters of the 3-DOF MMG model are estimated by minimizing the sum of squares of the errors between observed and predicted outputs as described by Ljung et al. [46]:

$$\underline{\varepsilon}(t) = \min_{\theta \in [\mathrm{LB}, \mathrm{UB}]} \sum_{t=1}^{\underline{N}} \left\| \underline{y}(t) - \hat{\underline{y}}(t) \right\|^2 \tag{35}$$

Here, $\underline{\varepsilon}(t)$ represents the prediction error, $\underline{N}$ represents the size of the training data, and $\|.\|$ indicates the 2-norm of a vector. Estimating the coefficients and parameters of the 3-DOF MMG mathematical models is often formulated as a nonlinear least-squares problem, which aims to fit predictions to observations in a given training set. The cost function of parameters, $V_{\underline{N}}(\theta, Z^{\underline{N}})$, of the nonlinear least squares problem without regularization is as follows [47]:

$$V_{\underline{N}}\left(\theta, Z^{\underline{N}}\right) = \frac{1}{\underline{N}} \sum_{t=1}^{\underline{N}} \frac{1}{2} \underline{\varepsilon}^2\left(t, \theta\right) \tag{36}$$

where $Z^{\underline{N}}$ is the training dataset. The regularised nonlinear least squares cost function is [48]:

$$\hat{V}_{\underline{N}}\left(\theta, Z^{\underline{N}}\right) = \frac{1}{\underline{N}} \sum_{t=1}^{\underline{N}} \frac{1}{2} \underline{\varepsilon}^2\left(t, \theta\right) + \frac{1}{\underline{N}} \lambda \left(\theta - \theta^*\right)^{\mathrm{T}} R \left(\theta - \theta^*\right) \tag{37}$$

where λ, R, and θ^* represent the regularization options of the grey box method in MATLAB. A higher value of the multiplication of λ and R reflects the confidence in the initial estimates of the parameters. `Nominal` selection keeps the estimated values close to their initial estimates. Eqs. (36) and (37) cannot be solved analytically in most cases and must therefore be solved iteratively using a numerical method such as the numerical minimisation path as follows [47]:

$$\hat{\theta}^{(i+1)} = \hat{\theta}^{(i)} + \alpha f^{(i)} \tag{38}$$

Here, $\hat{\theta}^{(i+1)}$ is the estimated parameter set at the $(i+1)^{\mathrm{th}}$ iteration, denoting the estimate of the minimization point. Meanwhile, α is a positive constant adjusted to obtain a reasonable decrease in $V(\theta)$, also known as the step size. $f^{(i)}$ is the search direction determined based on the information from previous iterations concerning $V(\theta)$, as stated by Ljung [47]:

$$f^{(i)} = -\left[V''\left(\hat{\theta}^{(i)}\right)\right]^{-1} V'\left(\hat{\theta}^{(i)}\right) \tag{39}$$

To determine the search direction f, common iterative search methods, known as Newton algorithms, use the gradient and the Hessian of $V(\theta)$. Various Newton optimisation algorithms, including adaptive Gauss-Newton (GNA) line search, gradient-descent (Grad) line search, sequential quadratic programming (fmincon), and Levenberg-Marquardt (LM) line search, are used in this study to minimise the cost function $V_{\underline{N}}(\theta, Z^{\underline{N}})$. The gradient of the cost function is, according to Ljung [37], as follows:

$$V'_{\underline{N}}\left(\theta, Z^{\underline{N}}\right) = -\frac{1}{\underline{N}} \sum_{t=1}^{\underline{N}} \underline{\psi}\left(t,\theta\right) \underline{\varepsilon}\left(t,\theta\right) \tag{40}$$

Here, $\underline{\psi}$ represents the gradient matrix of the cost function $V_{\underline{N}}$. To minimize $V_{\underline{N}}$, the search routine outlined by Ljung [47] iteratively proceeds as follows:

$$\hat{\theta}_{\underline{N}}^{(i+1)} = \hat{\theta}_{\underline{N}}^{(i)} - \mu_{\underline{N}}^{(i)} \left[R_{\underline{N}}^{(i)} \right]^{-1} V'_{\underline{N}}\left(\hat{\theta}_{\underline{N}}^{(i)}, Z^{\underline{N}}\right) \tag{41}$$

where $\hat{\theta}_{\underline{N}}^{(i)}$ is the i^{th} iteration, while $\mu_{\underline{N}}^{(i)}$ is the step size to minimize the cost function $V_{\underline{N}}$. $R_{\underline{N}}^{(i)}$ is a (d,d) - matrix and modifies the search direction. The Hessian of the cost function is [47]:

$$V''_{\underline{N}}\left(\theta, Z^{\underline{N}}\right) \approx \frac{1}{\underline{N}} \sum_{t=1}^{\underline{N}} \psi\left(t,\theta\right) \underline{\psi}^{\mathrm{T}}\left(t,\theta\right) \triangleq H_{\underline{N}}\left(\theta\right) \tag{42}$$

Once the `gna` line search method is selected in MATLAB, eigenvalues of the Jacobian matrix that are less than a certain threshold are neglected. $R_{\underline{N}}^{(i)}$ as follows, according to Ljung [47]:

$$R_{\underline{N}}^{(i)} = H_{\underline{N}}\left(\hat{\theta}_{\underline{N}}^{(i)}\right) \tag{43}$$

Here, $H_{\underline{N}}$ denotes Hessian, which is the second-order partial derivatives matrix. Eq. (43) is inserted back into Eq. (41), and the `gna` search routine can be written as [47]:

$$\hat{\theta}_{\underline{N}}^{(i+1)} = \hat{\theta}_{\underline{N}}^{(i)} - \mu_{\underline{N}}^{(i)} \left[H_{\underline{N}}\left(\hat{\theta}_{\underline{N}}^{(i)}\right) \right]^{-1} V'_{\underline{N}}\left(\hat{\theta}_{\underline{N}}^{(i)}, Z^{\underline{N}}\right) \tag{44}$$

When the `grad` line search method is selected in MATLAB, the matrix $R_{\underline{N}}^{(i)}$ is formed as follows, according to Ljung [47]:

$$R_{\underline{N}}^{(i)} = I \tag{45}$$

where I is the identity matrix, Eq. (45) is reinserted into Eq. (41), and the `grad` line search routine is simplified as follows [47]:

$$\hat{\theta}_{\underline{N}}^{(i+1)} = \hat{\theta}_{\underline{N}}^{(i)} - \mu_{\underline{N}}^{(i)} \left[I \right]^{-1} V'_{\underline{N}}\left(\hat{\theta}_{\underline{N}}^{(i)}, Z^{\underline{N}}\right) \tag{46}$$

Once the `lm` line search method is selected in MATLAB, which is a combination of the Gauss-Newton and Grad methods, the matrix $R_{\underline{N}}^{(i)}$ from Ljung [37] is:

$$R_{\underline{N}}^{(i)}\left(\lambda\right) = H_{\underline{N}}\left(\hat{\theta}_{\underline{N}}^{(i)}\right) + \lambda I \tag{47}$$

where λ is a positive scalar that is increased until a lower value of the criterion is found. Eq. (47) is inserted back into Eq. (41), and the `lm` search routine can be written [47]:

$$\hat{\theta}_{\underline{N}}^{(i+1)} = \hat{\theta}_{\underline{N}}^{(i)} - \left[H_{\underline{N}}\left(\hat{\theta}_{\underline{N}}^{(i)}\right) + \underline{\lambda} I \right]^{-1} V'_{\underline{N}}\left(\hat{\theta}_{\underline{N}}^{(i)}, Z^{\underline{N}}\right) \tag{48}$$

Increasing the value of λ results in a decrease in step size and a change in the search direction towards the gradient. When the `lsqnonlin` TRR search method is selected in MATLAB trust-region to the act of approximating the cost function [49], the general form for iterative search algorithms in Eq. (38) is rewritten as follows:

$$\hat{\theta}_{k+1} = \hat{\theta}_k + \alpha_k s_k \tag{49}$$

Here, α_k represents the step size, while s_k represents the search direction. However, unlike other Newton line search methods, determining the second term of Eq. (49) is not easily expressed in closed form. The TRR method has an advantage in handling constraints compared to other line search methods, as stated in [47]. For a detailed algorithm of the TRR method, refer to the studies of Coleman and Li [50], Zhang and Zhang [51], and Gao et al. [52].

3.3 Evaluation metrics of the system identification method

Evaluating different models against each other is an essential step in SI. While visual inspection of the results can be helpful, quantitative assessment through numerical calculations is often preferred. One of these calculations, the normalized root mean squared error (NRMSE), is given in [47] as follows:

$$\text{NRMSE} = \frac{\left\| \underline{y} - \underline{\hat{y}} \right\|}{\left\| \underline{y} - \underline{\bar{y}} \right\|} \tag{50}$$

where $\underline{\bar{y}}$ is the mean of the measured output data, this NRMSE assessment provides a measure between 0 and 1 that indicates the similarity between the predicted and actual output data. A value of 0 indicates a perfect match between the prediction and the actual data. For measuring errors and model precision, the other calculation method is the mean squared error (MSE) as follows in [47]:

$$\text{MSE} = \frac{1}{\underline{N}} \sum\nolimits_{t=1}^{\underline{N}} \frac{1}{2} \underline{\varepsilon}^T \left(t, \theta\right) \underline{\varepsilon}\left(t, \theta\right) \tag{51}$$

Therefore, using Eq. (51) aims to find a model whose complexity gives the lowest combined model variance and bias. In addition, a calculation method is used to assess the quality of the models, which is Akaike's final prediction error (FPE) as described in [47]:

$$\text{FPE} = \frac{1 + \dfrac{\underline{n}_p}{\underline{N}}}{1 - \dfrac{\underline{n}_p}{\underline{N}}} \frac{1}{\underline{N}} \sum\nolimits_{t=1}^{\underline{N}} \frac{1}{2} \underline{\varepsilon}^2 \left(t, \hat{\theta}_{\underline{N}}\right) \tag{52}$$

Here, $\underline{n}_p$ denotes the number of parameters to be identified in the model. It also includes the number of estimated initial states. FPE is a metric for assessing the expected performance of a model on validation data. Pillonetto et al. [45] also give the Bayesian information criterion (BIC), also known as the minimum description length:

$$\text{BIC} = \underline{N} \log \det \left[\frac{1}{\underline{N}} \sum\nolimits_{t=1}^{\underline{N}} \frac{1}{2} \underline{\varepsilon}^T \left(t, \theta\right) \underline{\varepsilon}\left(t, \theta\right) \right] + \underline{N} \left(\underline{n}_y \log\left(2\pi\right) + 1 \right) + \underline{n}_p \log\left(\underline{N}\right) \tag{53}$$

where $\underline{n}_y$ is the number of outputs of the model. The last method presented in this study is the corrected Akaike information criterion (AICc) instead of the commonly used AIC, which is defined by Pillonetto et al. [45] as follows:

$$\text{AICc} = \underline{N} \log \det \left[\frac{1}{\underline{N}} \sum\nolimits_{t=1}^{\underline{N}} \frac{1}{2} \underline{\varepsilon}^T \left(t, \theta\right) \underline{\varepsilon}\left(t, \theta\right) \right] + 2\underline{n}_p + \underline{N} \left(\underline{n}_y \log\left(2\pi\right) + 1 \right) + 2\underline{n}_p \frac{\left(\underline{n}_p + 1\right)}{\left(\underline{N} - \underline{n}_p - 1\right)} \tag{54}$$

Once the dataset size $\underline{N}$ is small, this criterion is often more reliable for selecting the best model with optimal complexity among the identified models.

3.4 Process of the system identification method

This paper presents a powerful method to determine the hydrodynamic coefficients and parameters of a 3-DOF digital MMG model. The key steps of the SI method are:

- Select the training data to be identified from the manoeuvres and create an `iddata` object providing the input data $\underline{u}$, which is the rudder angle of the ship δ, and the output data $\underline{y}$, which are the velocity components u, v, and r, as well as specifying the sampling interval.
- For the representation of the ship's dynamics, construct the `idnlgrey` model based on physical knowledge of the 3-DOF motion in the following way:
  (1) Describe the ship dynamics, represented by the 3-DOF motion equation in matrix form, as a set of first-order differential equations in a function within a Matlab M-file named `Ship.m`.
  (2) Specify the number of model outputs and the states and the number of model inputs.
  (3) Define the matrix θ, which consists of the coefficients and parameters of the 3-DOF MMG model, along with its boundaries b_i.
  (4) Define the initial states of the velocity components u, v, and r to represent the initial conditions at the start of the ship manoeuvring problem.
  (5) Define the `idnlgrey` model using the `Ship.m` file, which represents the state space of the 3-DOF MMG Model.
- To apply an offline grey box identification method, follow these steps:
  (1) Create an estimation option set that specifies the search method of the grey box algorithm, regularization options, maximum iteration number, and gradient options.
  (2) Use the `nlgreyest` (or `pem`) command and `lsqnonlin` search method to estimate the parameters of `idnlgrey` model.
- To compare the response of the `idnlgrey` models to the training and validation data as follows:
  (1) Use the `goodnessOfFit` command to check for errors and model precision by examining the NRMSE and MSE.
  (2) Continue the estimate by making a second call to `nlgreyest` (or `pem`) to improve the response of the `idnlgrey` models. Starting with TRR (`lsqnonlin`) and then applying GNA (`gna`), Grad (`grad`), SQP (`fmincon`), and LM (`lm`). Also implementing regularization options `Lambda`, `R`, and `Nominal` following TRR.
  (3) Select `idnlgrey` model based on the fit criteria (FPE, AICc, BIC) of models.

4. Numerical results and discussion

The mathematical model and process of SI, as described in the previous sections 2 and 3, have been applied to predict the manoeuvring performance of a full-scale KVLCC2 tanker and a scaled-model car carrier. The tanker, described in detail by Yasukawa and Yoshimura [14], is a 320 m full-scale ship. The car carrier, on the other hand, is a 4 m length model ship. Table 1 shows the principal geometric particulars of both ships.

Table 2 shows the main specifications of single propeller single rudder ships. These ships are equipped with a right-handed single-screw with four blades. It should be noted that open-water tests for the propeller of the car carrier model used in this study have not been conducted at BSHC.

Table 1 Nondimensional principal particulars of ships

Description with symbol	KVLCC2	Car Carrier	Unit
Ship length between perpendiculars, L, to beam, B, ratio	5.5200	6.0000	[-]
Beam, B, to draught, d, ratio	2.7900	3.0000	[-]
The profile area of the movable part of the rudder, A_R, to multiplied by the length, L, and draught of the ship, d, ratio	0.4400	0.0200	[-]
Block coefficient, C_B	0.8098	0.7360	[-]
Coordinate point of the centre of gravity, x_G, to Length, L, ratio	0.0350	-0.0140	[-]

Table 2 Main specifications of propeller

Parameters	KVLCC2	Car Carrier	Unit
Number of propeller blades, Z	4	4	pcs.
Diameter, D_P	9.860	0.132	m
Pitch ratio, P/D_P	0.721	0.926	[-]
The blade area ratio, A_E/A_0	0.431	0.615	[-]
Propeller revolution, n	1.53	13.55	[1/s]

The study tested a benchmark tanker and a car carrier for calm water manoeuvres. The training data for the full-scale tanker's zigzag manoeuvres, with rudder angles $-20°/+20°$, were obtained using the open-source simulation tool MANSIM [38]. The validation study of TRR method was performed using the free-running results of the 1/45.7 scaled model tanker conducted by Maritime Research Institute Netherlands (MARIN) for The Workshop on Verification and Validation of Ship Manoeuvring Simulation Methods (SIMMAN 2008) [39]. The verification study of TRR method was performed using the car carrier. The free-running tests of the car carrier with a NACA 0012 profile were carried out in the BSHC test basin, which measures 60 x 40 x 2.5 m. Standard manoeuvres suggested by IMO were performed in calm water conditions, with a water depth set to a depth/draught (h/d) value of 2.00. Table 3 shows that the model test data are divided into training, validation, and verification sets. The training set consisted of the zigzag $+20°/-20°$ tests proposed in Källström's [19] thesis study, while the verification set included the turning circle, pull-out, and spiral tests. The free-running test and simulation data were collected using a time series, which recorded the trajectory, total ship speed, heading angle (ψ), rudder angle (δ), yaw rate (r), and propeller speed at 0.100 and 0.136 (sec) sampling intervals for car carrier and KVLCC2, respectively. While the tests and simulations of the car carrier's free-running model maintained a constant forward speed of 1.20 (m/s), assuming a constant propeller speed, the simulations of the KVLCC2 maintained a forward speed of 7.90 (m/s). The steering rate is set to 2.34 (°/sec) for the full-scale ship KVLCC2 and 16.26 (°/sec) for the car carrier in the model simulation tests.

4.1 Application of system identification to KVLCC2 and car carrier

The authors of this study suggested that linear derivatives are estimated more accurately in zigzag tests as the data is more linear than in the turning circle test, which is a non-linear manoeuvre. This impact is particularly pronounced in unsteady-state conditions typical of zigzag tests, requiring more precise estimations. The authors initially used the TRR method and then applied various line search methods to obtain a model, as the line search algorithm cannot handle bound constraints. The linear and nonlinear derivatives were estimated with these models, using the zigzag test data listed in Table 3 for Manoeuvre No. 1.a and 1.b for the KVLCC2 and car carrier, respectively. The required information, such as hydrodynamic derivatives

and parameters, for simulating Manoeuvre No. 1.a for the KVLCC2 tanker was obtained from the literature [38]. This includes the main dimensions, hydrodynamic properties and derivatives, propeller, and rudder parameters. The TRR method was used to identify the parameter matrix, θ, for the simulation of Manoeuvre No. 1.a. of the KVLCC2 tanker. Furthermore, the TRR method and varied line search methods were used to determine the parameter matrix θ, for the simulation of Manoeuvre No. 1.b. of car carrier. Here,

$$\theta = \left[-X_0' \;\; X_{vv}' \; X_{vr}' \; X_{rr}' \; X_{vvvv}' \; Y_v' \; Y_r' \; Y_{vvv}' \; Y_{vvr}' \; Y_{vrr}' \;\; Y_{rrr}' \; N_v' \; N_r' \; N_{vvv}' \; N_{vvr}' \; N_{vrr}' \; N_{rrr}' \right]^{\mathrm{T}} \text{ for KVLCC2 tanker and}$$

$$\theta = \begin{bmatrix} -X_0' \;\; X_{vv}' \; X_{vr}' \; X_{rr}' \; X_{vvvv}' \; Y_v' \; Y_r' \; Y_{vvv}' \; Y_{vvr}' \; Y_{vrr}' \;\; Y_{rrr}' \; N_v' \; N_r' \; N_{vvv}' \; N_{vvr}' \; N_{vrr}' \; N_{rrr}' \; l_r' \\ \varepsilon \; m_x' \; m_y' \; J_z' \; t_R \; a_H \; x_H' \; t_P \; w_{P0} \; \gamma_{R_{upper}} \; \gamma_{R_{lower}} \end{bmatrix}^{\mathrm{T}} \text{ for car carrier.}$$

Table 3 Experimental & simulation test program of car carrier model

Manoeuvre No.	Ship Type	Manoeuvre Type	Propeller speed (rpm)	Commanded rudder angle (deg)	*Fr* [-]	Data type
1.a	KVLCC2	Zigzag	91.8	−20° / +20°	0.142	Training, Validation
1.b	Car carrier	Zigzag	813	+20° / −20°	0.194	Training
2.a	Car carrier	Turning Circle	813	+35°	0.194	Verification
2.b	Car carrier	Turning Circle	813	−35°	0.194	Verification
3.a	Car carrier	Pull out	813	+25° / −5°	0.194	Verification
3.b	Car carrier	Pull out	813	−25° / +4°	0.194	Verification
4	Car carrier	Spiral	813	+35° / −35°	0.194	Verification

Accurately estimating initial parameters is crucial for commencing the model estimation process. To achieve more precise outcomes, it is recommended to impose upper and lower constraints on the parameter range with values closer to the actual value rather than using the default range of $+\mathrm{Inf}/-\mathrm{Inf}$, as initially proposed by Ljung [49]. The authors of this study restricted the values of the hydrodynamic coefficient and parameters to realistic limits. The boundaries of coefficient and parameters for deep water were established according to Yoshimura's [53] and Yoshimura and Masumoto's [40] studies, as presented in Table A.1 for KVLCC2. Assuming that the ratio h/d 2.00, which is between 1.5 and 3.0 in this study, represents medium deep water, the deep water to shallow water transition formulas specified in Taimuri et al.'s [54] study were applied, and the boundaries estimated by transition formulas of the coefficients and parameters were presented in Table A.1 for car carrier. The parameter estimation process started with initial numerical values given in Tables A.1 and A.2 in Appendix 1 for car carrier and KVLCC2 respectively and ended with fine-tuning of the parameters given in Tables A.2 and A.3 for KVLCC2 and car carrier respectively.

4.2 Numerical results

Once determining the coefficients and parameters of the mathematical model, `idnlgrey` models were created in the MATLAB environment, simulation studies were performed for the KVLCC2 tanker and car carrier. For this purpose, the grey box model was selected in the System Identification Toolbox library of the MATLAB/Simulink Library Browser. Then, the `idnlgrey` model from the MATLAB environment was embedded into the grey-box model in the MATLAB/Simulink environment as described by Ljung et al. [55]. Fig. 3 shows the scheme of the car carrier created by the authors of this study and used for simulation studies in MATLAB/Simulink. The ship's trajectory and heading angle were derived by the simulation model at each time step by processing three velocities. `The ode45` function was used as the ordinary differential equation solver. The simulation tests by the scheme shown in Fig. 3 were performed on two computers equipped with

Windows 10 operating system. The specifications of the first computer are as follows: Intel(R) Core (TM) i7-8750H processor with a speed of 2.20 GHz and 16 GB of memory. The second computer is equipped with an AMD Ryzen 9 3950X 16-Core Processor with a speed of 3.50 GHz and 64 GB memory.

The time-dependent rudder command for the zigzag test of the KVLCC2 tanker and the car carrier was generated using the block of `zigzag test rudder command` with `fin/rudder machinery` from the Marine GNC Toolbox developed by Fossen [56], presented by Perez and Blanke [57] and evaluated by Perez et al. [58] library of the MATLAB/Simulink Library Browser, as shown in Fig. 4.

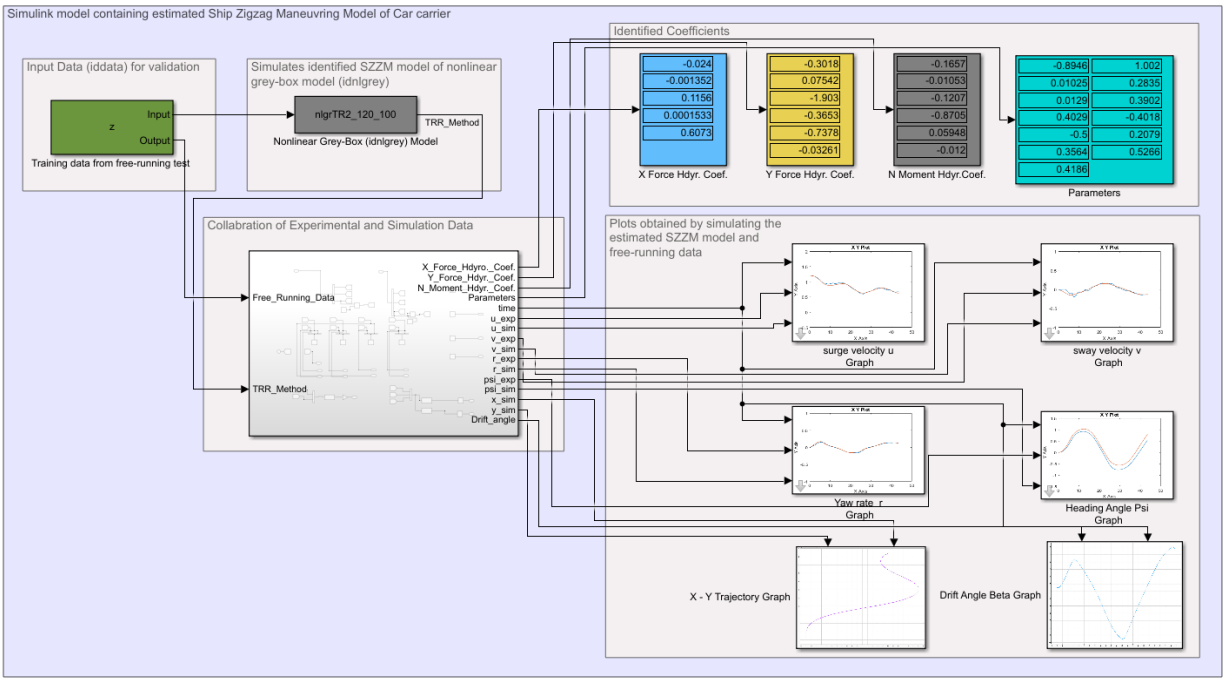

Fig. 3 Simulation environment of the identified digital model with block diagram in MATLAB/Simulink

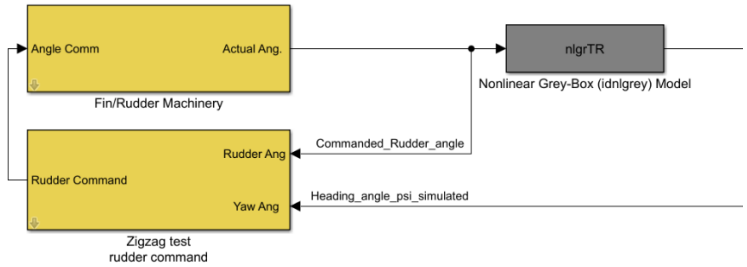

Fig. 4 Identified digital model with zigzag test rudder command block in MATLAB/Simulink

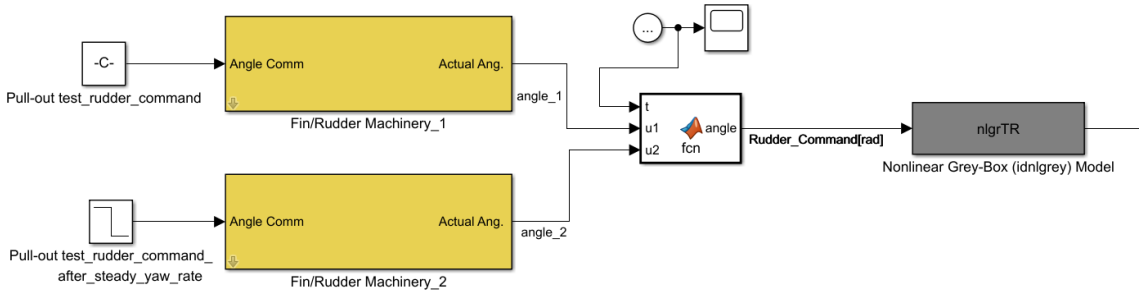

Fig. 5 Identified digital model with fin/rudder machinery block in MATLAB/Simulink

The `fin/rudder machinery` block was also utilized to produce rudder commands for the turning circle, pull-out, and spiral tests for the car carrier. As stated in [59], `MATLAB Function` block is used to implement command rudder angle at the beginning and when the ship's yaw rate reaches a steady state.

Fig. 5 displays the `fin/rudder machinery` block that was used in the pull-out test carried out in this study.

4.2.1 Application of system identification to KVLCC2 and results

The results obtained by applying the grey box identification method to determine the hydrodynamic derivatives of the 3-DOF manoeuvring motion are summarized for KVLCC2. All the necessary information for the simulation, including the propeller and rudder parameters for KVLCC2, was obtained from the literature [38]. The list of hydrodynamic derivatives from the application of SI to KVLCC2 is given in Table A.2 in Appendix 1.

In this study, it was investigated whether the identification results could be improved by using the adjustment interval instead of the $[-\text{Inf}, +\text{Inf}]$ value. Three models, IV 101, IV 102, and IV 103, were created for this purpose. The adjustment interval of IV 101 is $[-\text{Inf}, +\text{Inf}]$, while that of IV 102 is similar to IV 101 except for the b_1 value $[-0.23, -0.21]$. Here, b_i is an adjustment interval while non-dimensional resistance coefficient X'_0 has a lower bound of -0.23 and an upper bound of -0.21. The adjustment interval of IV 103 is given in Table A.2. Analysis of the result of $-20°/+20°$ zigzag test identification showed that reasonable estimates were obtained from the non-linear models IV 101 and 102. However, the results were slightly improved by implementing the adjustment interval to the nonlinear model IV 103. The simulations of the three obtained models were compared with MARIN's result given for SIMMAN [39] and with MANSIM [38] references. The reference data [39] were obtained from MARIN's 1/45.7 scale free-running model tests. The MANSIM tool [38] was used to perform full-scale simulations and obtained the results. The heading angle prediction performance of all identified models is illustrated in Fig. 6. SB represents system-based prediction as system identification in Fig. 6. As a consequence of SI implementation, for models IV 101 and IV 102, it was found that the signs of the non-linear derivatives changed with respect to the actual value, but that the linear coefficients did not change their signs, which made it possible to determine them more precisely. Moreover, in the comparisons made between the three models, it was found that the IV 101 and 102 had the lowest N'_r value given in Table A.2, which was calculated to be -0.0356 for IV 101 and 102 models. These two models had the highest first overshoot angle (OS) of the same value of -37.73 (deg) as shown in Fig. 6. However, in Table A.2, model IV 103 was found to have the lowest N'_v value and the lowest first OS of -34.29 (deg) as shown in Fig. 6. As a result, while the criteria with the lowest AICc and BIC values indicated that models IV 101 and 102 were preferable to model IV 103 as shown in Table A.4, model IV 103 was captured first and second OS very close to the MARIN's result given for SIMMAN [39]. This is confirmed by the NRMSE value of the yaw rate for model IV 103 as given in Table A.5.

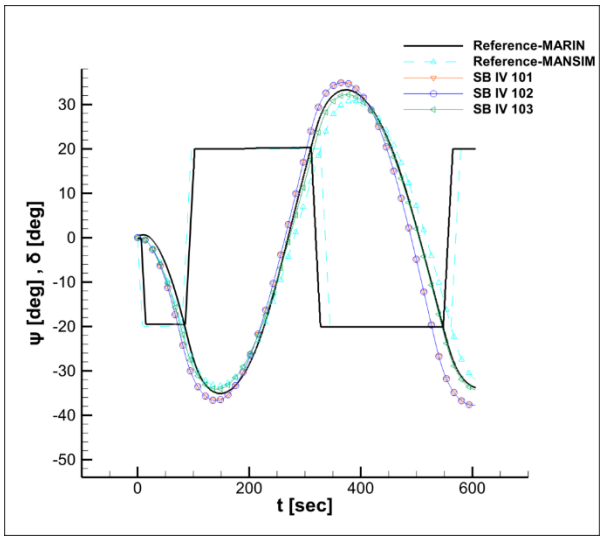

Fig. 6 Comparison of t [sec] versus Heading ψ [deg]between the free-running model test of KVLCC2 and simulation with the identified model during a $-20°/+20°$ zigzag test Manoeuvre No. 1.a

4.2.2 Application of system identification to car carrier and results

The results obtained from applying the grey box identification method with the varied search algorithms to determine the hydrodynamic properties and derivatives of the 3-DOF manoeuvring motion are summarized for the car carrier in Table A.1. Five models, IV 201, IV 202, IV 203, IV 204, and IV 205, were created for this purpose. After performing a simulating Manoeuvre No. 1.b $+20°/-20°$ zigzag test for the car carrier by using the simulation environment created by the authors in this study, shown in Fig. 3, the prediction accuracy of the digital models was compared. Poor estimates were generally obtained from models with line search directions, IV 202, IV 203, IV 204, and IV 205. An illustration of the results obtained by simulation with identified models is shown in Fig. 7. It can be seen that there are significant differences between IV 201 and other models. The model selection scores of the identified model with the TRR method, as well as the values of MSE and NRMSE for the surge and sway velocity, are differ from the KVLCC2 results; they are higher, as described in Table A.6. The reason can be that the training data of the KVLCC2 tanker was better than the car carrier model. The error results of IV 201 were the best among models IV 202, IV 203, IV 204, and IV 205 with the lowest AICc, BIC, and FPE values as shown in Table A.7. It can also be concluded from Fig. 7 that the phase shifts in heading angles are generally caused by the mismatch in rudder execution times.

Besides the option of various search algorithms, one of the estimation options of the grey box algorithm is the regularization option, which contains three terms, λ, R, and θ^*, defining the penalty term used. The penalty term θ^* with `Nominal` command is selected as `model`. A list of candidates λ and R values was generated to be tested. The TRR model with regularization options was estimated for each candidate set of regularization constants, and the models were compared to the validation data to determine if they fit. It is assumed that the value of the linear coefficients is more reliable than the non-linear coefficients to remain close to the initial guess. A higher value of the multiplication of λ and R was kept very close to the initial value of the parameters as stated [47]; it was concluded with a lower percentage fit to the validation data, such as for the drop in sway velocity from 75% to 50% as shown in Fig. A1 in Appendix 1. Thus, λ was set to 1.20, R was set to 1.00 for linear coefficients and 0.001 for non-linear coefficients, and a variant of model IV 201 was created with these regularisation options and named model IV 211. Furthermore, upon analysis of the predictions in the IV 211 model, which were obtained by applying regularization to the IV 201 model, it was observed that there was no additional improvement according to the model selection scores given in Table A.7. However, it can be seen that there is an improvement in predicting the yaw rate, as shown in Table A.6.

It was observed that the prediction results of the IV 202, IV 203, IV 204, and IV 205 models were worse compared to IV 201, in Fig. 7.a and the fit criteria in Tables A.6 and A.7. For this reason, it was decided to perform the identification with model IV 201 before these methods and then apply these methods sequentially. In this way, four more different models were obtained, named IV 212, IV 213, IV 214, and IV 215. It can be seen that the improved variant of IV 201 significantly reduces the value of the MSE of the identified models IV 212, IV 213, IV 214, and IV 215 with the line search method compared to their initial models IV 202, IV 203, IV 204, and IV 205, as shown in Tables A.6 and A.7. Although the criterion with the lowest value of AICc and BIC indicated that model IV 212 was preferable among the other models, as shown in Table A.7, model IV 215 was captured first OS very close to the free manoeuvring data of Manoeuvre No. 1.b as shown in Fig. 7.b. This is supported by the NRMSE value of the yaw rate for model IV 215, as given in Table A.6. Approximately the closest accuracies were thus obtained from the models combined with model IV 201. While EFD represents free-running data, SB represents system-based prediction as system identification in the following figures.

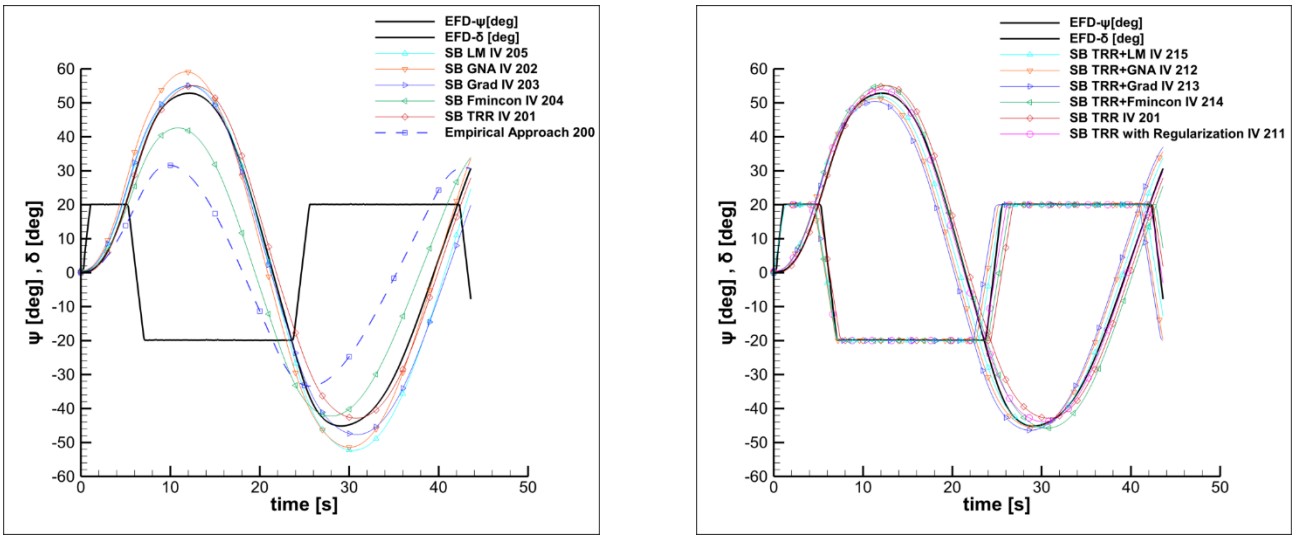

(a) Time series t [sec] versus Heading ψ [deg], initial (b) Time series t [sec] versus Heading ψ [deg], final

Fig. 7 Comparison of time series between the free-running model test and simulation with the identified model varied search method during a $+20° / -20°$ zigzag test Manoeuvre No. 1.b

4.2.3 Verification results of identified models for car carrier

Five simulations of IMO standard manoeuvres listed in Table 3, including turning circle, pull-out, and spiral tests, were each performed at constant speed for the car carrier. The free-running manoeuvre test data confirmed the verification of this method. These simulations utilizing the scheme shown in Fig. 3 used the updated parameters as given in Table A.1 for model IV 201 and Table A.3 for models IV 211, IV 212, IV 213, IV 214, and IV 215. Figs. 8, 9, and 10 show graphical comparisons of the free-running model with the simulation results for Manoeuvre No. 2.a and 2.b. It can be seen that the simulation results with identified models did not differ significantly. Based on all turning circle simulations, it was concluded that both the steady yaw rate and trajectory were predicted close to the free-running test data once the IV 213 was used instead of model IV 201. However, it was found that model IV 201, identified by the TRR method, was the best at predicting the speed of the ship model as shown in Figs. 8 and 9.

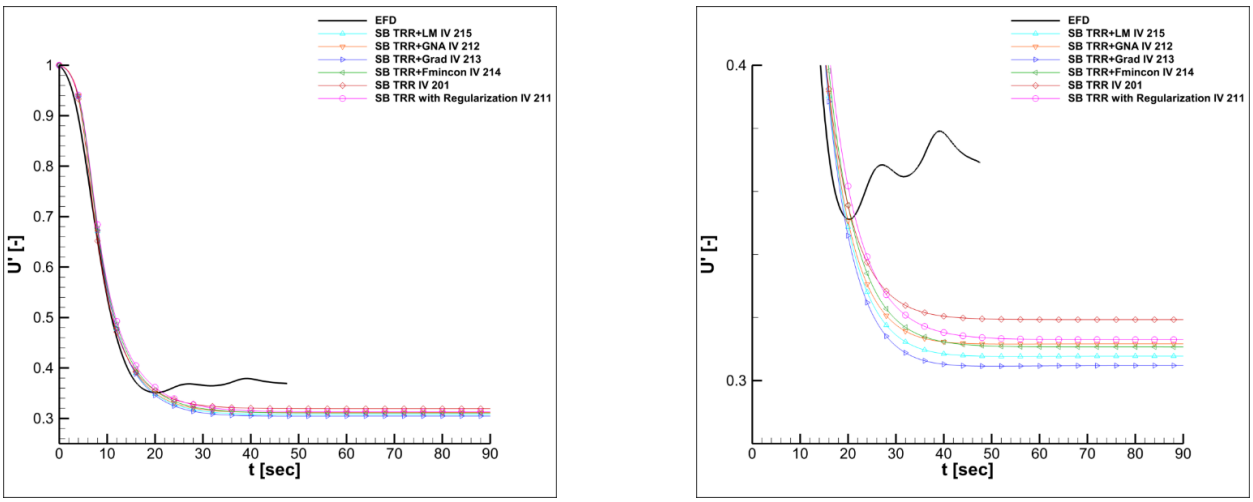

Fig. 8 Comparision of the time series t [sec] versus ship speed U [-] at Maneuver No. 2.a (turning circle with rudder angle set on $+35°$) measured in free-running model test and simulation by identified models. An enlarged version is shown on the right.

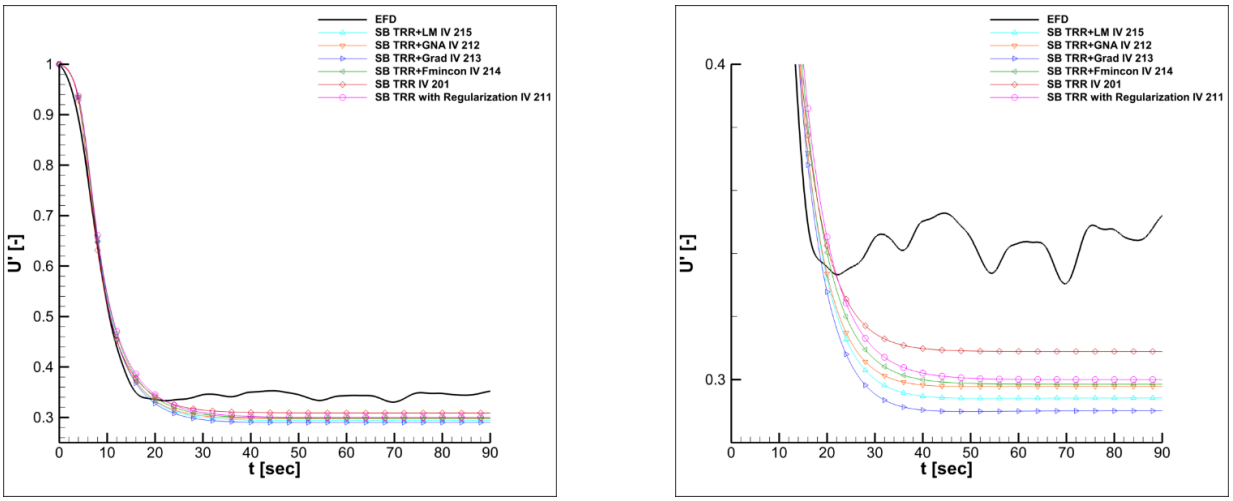

Fig. 9 Comparision of the time series t [sec] versus ship speed U [-] at Maneuver No. 2.b (turning circle with rudder angle set on $-35°$) measured in free-running model test and simulation by identified models. An enlarged version is shown on the right.

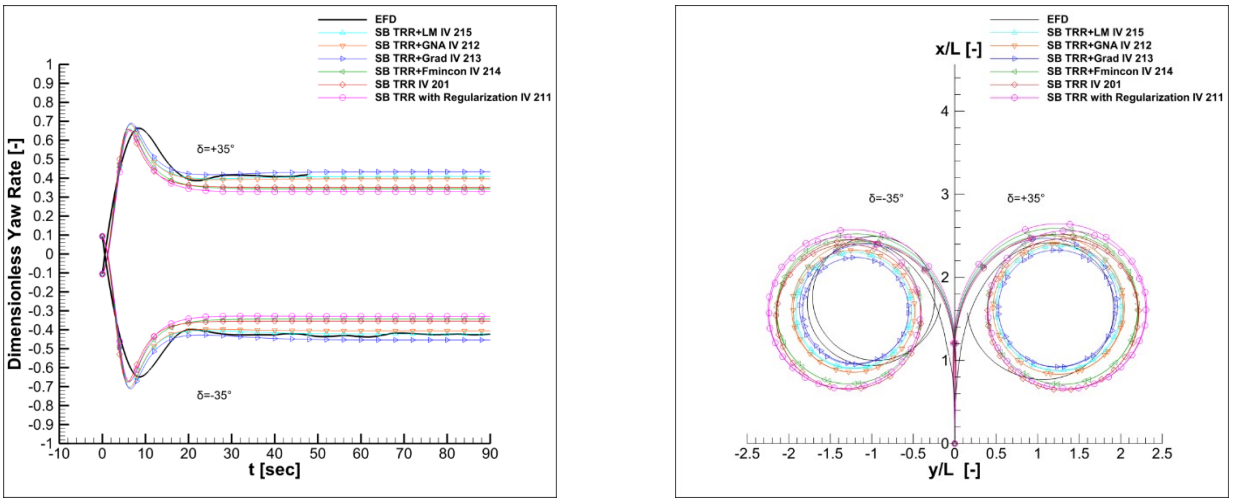

(a) Time series t [s] versus Yaw rate r [-] (b) Trajectory $y/L - x/L$ [-]

Fig. 10 Comparision of the yaw rate and turning trajectory at Maneuver No. 2.a and 2.b (turning circle to both sides) measured in free-running model test and simulation by identified models.

Table 4 compares the non-dimensional turning indices, including advance ADV, transfer TR, tactical diameter TD, and drift angle at $360°$ β of the models identified for the car carrier. Once the models were examined, it can be concluded that ADV and TD values for Maneuver No. 2.a were lowest in model IV 213, which had the lowest Y'_v value in Table A.3. Also, it can be deduced from Tables 4 and A.3 that a reduction in the magnitude of N'_v can worsen some of the manoeuvring indices, such as the advance and transfer diameter of the turning circles. For example, model IV 211 has the lowest magnitude of N'_v in Table A.3 with -0.1657 given and the highest indices ADV and TD.

Graphical comparisons of the free-running model with the simulation results are shown in Fig. 11 for Manoeuvre 3, a pull-out test to indicate the ship's straight-line stability quickly. The simulation results with the identified models do not vary much. On the basis of both side-pull simulations, it was concluded that both the yaw rate and trajectory were predicted close to the free-running test data when model IV 213 was used instead of model IV 201. However, it was found that model IV 201, as identified by the TRR method, was the best at predicting the speed of the ship model as shown in Figs. 11.a and 11.b, similar to the turning test. It can also be concluded from Figs. 11.a, 11.b and 11.c that the phase shifts in ship speed and yaw rate from steady state to the end of the test are generally due to a mismatch in the time to execute the steering commands.

Table 4 Simulation results of turning indices

Indices	Measured	Identified Version					IMO
	Model # 200	Model # IV 201	IV 211	IV 212	IV 213	IV 214	IV 215	
ADV / L, $\delta = 35°$	2.3821	2.4769	2.5990	2.4655	2.4383	2.5408	2.4714	< 4.50 L
TD / L, $\delta = 35°$	1.8923	2.1773	2.2600	2.0098	1.9330	2.1627	1.9908	< 5.00 L
TR / L, $\delta = 35°$	0.9179	0.9201	0.9200	0.8634	0.8562	0.8900	0.8553	-
β at 360°	15.2962	16.6637	18.5609	16.2089	14.6498	18.3684	15.7484	-
ADV / L, $\delta = -35°$	2.3744	2.4097	2.5238	2.3935	2.3666	2.4768	2.4008	< 4.50 L
TD / L, $\delta = -35°$	-1.7590	-2.1148	-2.1954	-1.9267	-1.8423	-2.0992	-1.9119	< 5.00 L
TR / L, $\delta = -35°$	-0.8538	-0.8912	-0.8905	-0.8323	-0.8250	-0.8727	-0.8251	-
β at 360°	-13.3562	-17.2190	-19.4226	-16.5925	-14.7321	-19.1371	-15.9556	-

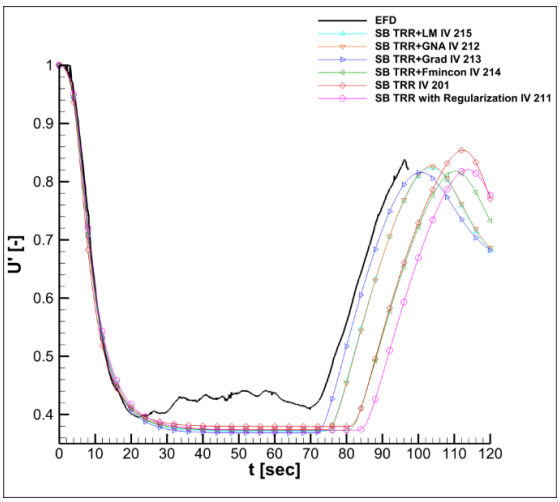

(a) Time series t [sec] versus ship speed U [-], portside

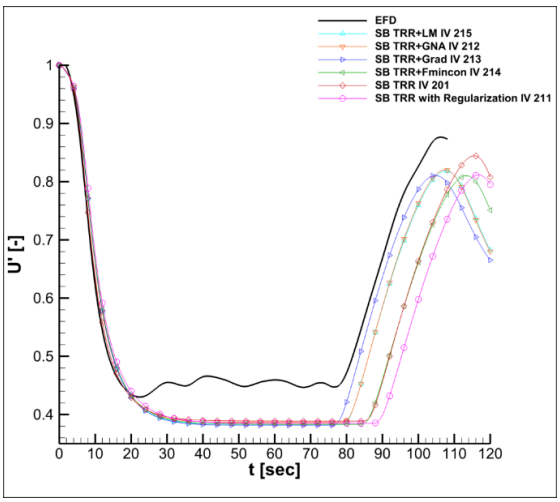

(b) Time series t [sec] versus ship speed U [-], starboard

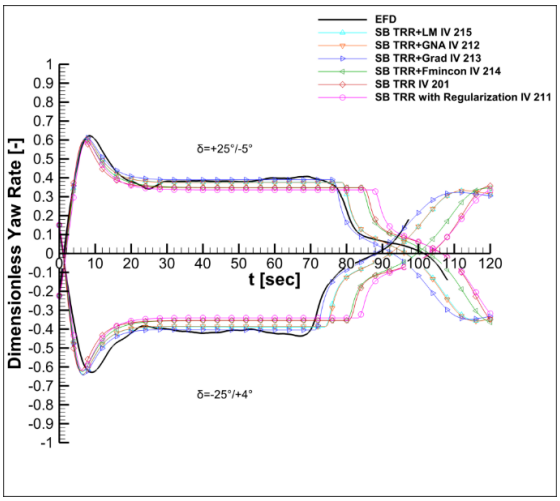

(c) Time series t [s] versus Yaw rate r [-]

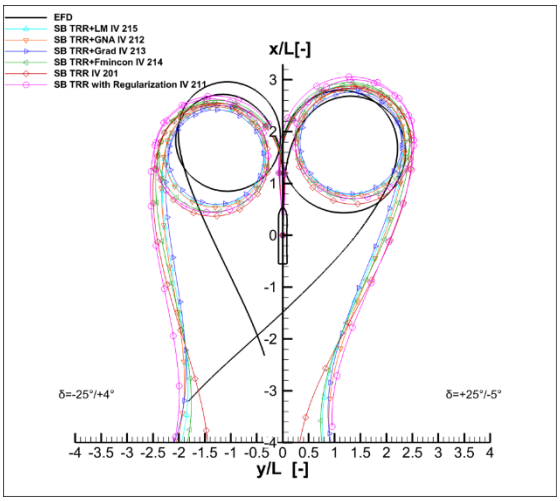

(d) Trajectory $y / L - x / L$ [-]

Fig. 11 Comparison of pull-out test case for car carrier, from simulation and free-running model test data of Manoeuvre No. 3

The digital model accurately captures the dynamics of the car carrier, as demonstrated by the turning circle and pull-out tests. IMO standards specify that the tactical diameter TD should not be more than five times the length of the ship; this study shows in Figure 10.b and Table 4 that both the free running test result of car carrier and the simulations with the identified digital models comply with this standard. The model demonstrated an asymmetry around the ship in its turning ability due to the screw propeller, despite the car carrier having a symmetric hull form and a symmetric NACA 0012 rudder profile. This resulted in a smaller diameter in the steady port side turn than in the starboard turn, as illustrated in Figs. 10.b and 11.d. This is further explored in Manoeuvre No. 4, where the spiral test simulation was initiated with the model on a straight course. The model's rudder was adjusted to approximately $+35°$ towards the starboard side and maintained until a steady yaw rate was achieved. While ITTC [5] recommends a maximum rudder angle of $+25°$, the rudder angle was subsequently reduced in $5°$ increments, and the process was repeated for both starboard and port sides up to $35°$. Fig. 12 illustrates the actual measured data of the spiral test and the results of the spiral test's simulations of the verification process, showing the response of the identified models to varying rudder angles. In the reverse spiral test, the width and height of the spiral loop were determined as shown in Fig. 12. Unlike the spiral test, instead of $5°$ rudder angle steps, the rudder was changed as decreasing $1°$ steps between $5°$ and $1°$, and $0.1°$ steps between $1°$ and amidships. This procedure was repeated from the counter-rudder port to the starboard side. The non-dimensional yaw rate in the spiral test was predicted to be closer to the free-running test data when model IV 213 was used instead of the IV 201 model. It is noteworthy that at a rudder angle (δ) of $0°$, the non-dimensional yaw rate (r') for the IV 213 model was 0.22, which is the closest value to the measured data of 0.170. The results of the spiral test and the pull-out manoeuvre indicate that the ship model exhibited poor course-keeping ability. Furthermore, the simulation of both spiral and reverse spiral test revealed that the yaw stability of the car carrier was low.

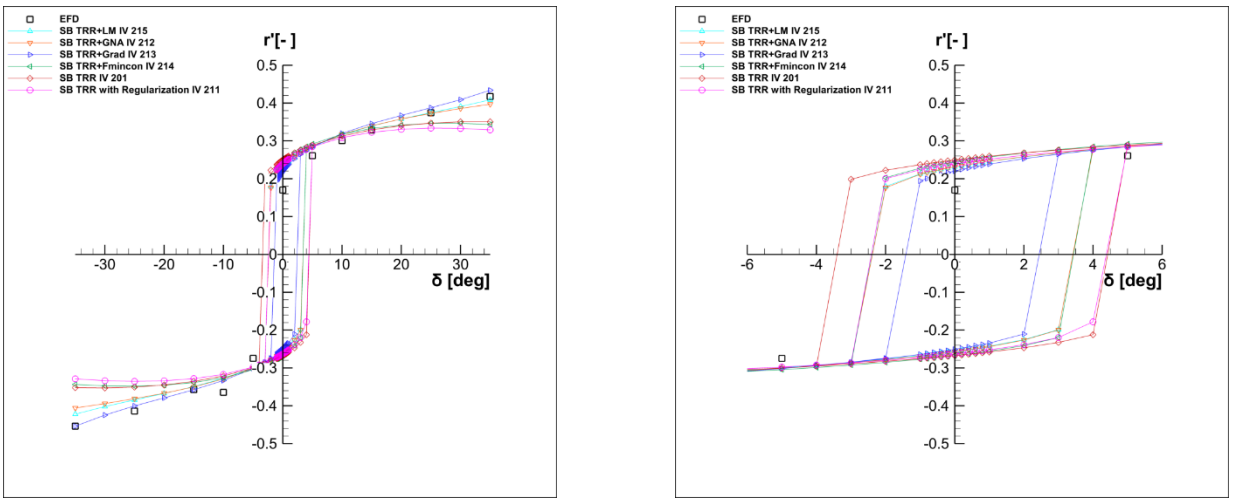

Fig. 12 Comparison of rudder angle δ [deg] versus yaw rate r [-] of simulated spiral manoeuvring test data and free-running test data of Manoeuvre No. 4. An enlarged version is shown on the right.

4.2.4 Assessment of straight-line stability

According to Sutulo and Guedes Soares [60], it has been proposed that there is a correlation between straight-line stability and overshoot angle. Therefore, in this study, an adverse case, a correlation between straight-line instability and high overshoot angle, was investigated. The manoeuvring performance of the car carrier was assessed according to the IMO [61] requirements. The first OS angle of the car carrier exceeded $+25°$ at the $+20°/-20°$ zigzag manoeuvre to assess the yaw checking and course-keeping ability of both actual measured data and identified models, as given in Table 5.

Table 5 1st OS angles of the car carrier in Zigzag $\delta = +20° / -20°$ Manoeuvre No. 1.b

	Measured	Predicted						Suggested by IMO
Model #	200	IV 201	IV 211	IV 212	IV 213	IV 214	IV 215	
1st OS	32.83°	35.04°	33.88°	31.31°	30.39°	35.17°	31.98°	< 25°

The straight-line stability, also known as the dynamic stability criterion, according to the studies of Kinaci and Ozturk [62], is as follows:

$$C = Y_v' \left(N_r' - m' x_G' \right) - N_v' \left(Y_r' - m' \right) > 0 \tag{55}$$

The index C was calculated, and the negative values in Table 6 show that the car carrier has inherent dynamic stability. Nevertheless, the first OS angle value in Table 5 of the car carrier is larger than the IMO requirements, which can result from the negative value of the index C. The dynamic instability finding was supported by Manoeuvre No. 3, the pull-out test results, as shown in Fig. 11, indicating the need for autopilot assistance in course-keeping. The amount of dynamic directional instability is also assessed by performing Manoeuvre No. 4, the spiral test, as shown in Fig. 12. Therefore, according to the findings of this study, there is a correlation between straight-line instability and high overshoot angle.

Table 6 Comparison of the car carrier stability index with models identified using data from Manoeuvre No. 1.b

	Predicted					
Model #	IV 201	IV 211	IV 212	IV 213	IV 214	IV 215
C [-]	-0.0313	-0.0257	-0.0290	-0.0260	-0.0297	-0.0284

5. Practical implications and future directions

In this study, the authors incorporated the SI method into the MMG mathematical model to achieve high accuracy. The authors implemented the MMG model of a car carrier and compared the results to data obtained from free-running tests performed at BSHC. The proposed methodology provides a reliable framework for accurately predicting and assessing the manoeuvring performance of car carrier by IMO criteria. In summary, this method is a reliable reference for establishing efficient manoeuvring performance in car carrier models for practical applications. The successful application of the grey-box method to the MMG model brings significant benefits to ship control systems and marine simulation environments. The precision of this method enhances the reliability of the MMG model in predicting ship manoeuvring, thereby facilitating more informed decisions in various operational conditions.

However, it is essential to note that the authors' analysis, while comprehensive, is based on specific manoeuvring data and may not encompass all possible scenarios or varying operational conditions. Future research should be extended to investigate the manoeuvring performance of car carriers in medium-deep water to extremely shallow waters, as well as different loading conditions. The results of future studies can be helpful in predicting the trajectory of the car carrier in the turning circle and predicting the OS angles of the zigzag manoeuvres for shipmasters and autonomous vessels. This is particularly relevant in inland waterways or ports where dredging and sediment removal, as mentioned in the study by Bose and Dhar [63], are regularly required to enable deeper draught ships to enter ports worldwide. In addition, incorporating roll motion into the model is essential, especially in scenarios where roll dynamics significantly affect manoeuvrability. These prospective studies will enhance the authors' understanding of ship behaviour under different conditions and a further improvement in the predictive accuracy and applicability of ship manoeuvring models. The authors will focus on digital twin technology, which allows for fully autonomous ship navigation through an online system identification method. They will also examine its control application, which is a crucial component of route tracking.

6. Conclusions

The study involved identification analysis and simulation of a benchmark tanker and a car carrier. The objective of this study was twofold: to investigate the feasibility of determining ship manoeuvring dynamics using system identification methods, and to evaluate the manoeuvring characteristics using experimental results compared to predicted results. The main conclusions are summarised below.

Experimental data for both ships were analysed in calm water. It was found that grey box modelling among system identification methods help predict ship manoeuvring dynamics and offer a good alternative to captive tests. Several alternative search methods of the grey box method were also created, analysed, and simulated. According to the simulation results of the obtained models, the combined TRR and Grad method was superior to the TRR method. It can be concluded that the grey box method discussed easily can be implemented on many types of ships, although both identifications so far have been performed with a benchmark tanker and a car carrier.

The authors' results show that the model effectively predicts the manoeuvring performance of a tanker and car carrier, specifically emphasizing on zigzag manoeuvres, turning circles, pull out test, and spiral test. The comparison of the simulation results with experimental data underscores the accuracy and effectiveness of the grey-box method in improving the predictive capabilities of the MMG model. The SI method can provide a speedy and cost-effective option for manoeuvring predictions. This approach is reliable for predicting ship motions in calm waters. It has significant implications for ship control systems and the simulation environments to improve marine safety. Key results indicate that the model's yaw-checking performance does not meet IMO criteria, resulting in straight-line instability. Additionally, the model exhibits inadequate course-keeping stability, readily observed from the simulation of pull-out and spiral tests using the MMG model based on the SI method. Moreover, there is a connection between inherent dynamic instability and large overshoot angle. The simulation results closely agree with actual manoeuvring data, confirming the identified models' accuracy and usefulness in estimating MMG model parameters.

Predicting the full-scale manoeuvrability of a ship using only scaled models is challenging. Sea trial data from the full-scaled ship can be integrated with model testing. It is nevertheless important to note that no correction for the scale effect was applied in the current study, and therefore, caution is advised when applying these results to estimate the manoeuvrability of a full-scaled car carrier.

Future studies should investigate the inclusion of roll motion and assess the effect of shallow water conditions on yaw control performance. These investigations will enhance researchers' understanding of ship manoeuvrability in various operational conditions.

Acknowledgements

The Scientific and Technological Research Council of Türkiye funding under grant 53325897-115.02-277670 and a Visiting Scholarship of Elis ATASAYAN at BSHC in IMSETHC BAS (Varna, Bulgaria) are acknowledged. Also, the multi-disciplinary project entitled "Prediction of Mission-Based Manoeuvring for Ships and Development of Manoeuvring Performance Based on Artificial Intelligence Algorithms" (Code: FCD-2022-4536) supported by the Scientific Research Projects Coordination Unit of Yıldız Technical University is gratefully acknowledged by the first and third authors.

REFERENCES

[1] Göksu, B., Bayramoğlu, K., 2023. Effect of Electric Vehicle Transportation and Carbon Capture System on Concept Ro-Ro Ship Stability and EEDI. *Marine Science and Technology Bulletin*, 12(3), 267–281. https://doi.org/10.33714/masteb.1313638

[2] Menges, D., Von Brandis, A., Rasheed, A., 2024. Digital Twin of Autonomous Surface Vessels for Safe Maritime Navigation Enabled through Predictive Modeling and Reinforcement Learning. *42nd International Conference on Ocean, Offshore and Arctic Engineering*, ASME 2023, 11-16 June, Melbourne, Australia, 86878, V005T06A025. https://doi.org/10.1115/OMAE2023-100626

[3] ITTC, 2005. The Manoeuvring Committee, Final Report and Recommendations to the 24th ITTC. *Proceedings of the 24th ITTC - Volume I*.

[4] Lyster, C. A., Knights, H. L., 1979. Prediction Equations For Ships' Turning Circles. *North East Coast Inst of Eng & Shipbuilders Trans*, 95(4).

[5] ITTC, 2017. Full Scale Manoeuvring Trials, 7.5-04-02-01. *ITTC - Recommended Procedures and Guidelines.*

[6] Araki, M., Sadat-Hosseini, H., Sanada, Y., Tanimoto, K., Umeda, N., Stern, F., 2012. Estimating Maneuvering Coefficients Using System Identification Methods with Experimental, System-Based, and CFD Free-Running Trial Data. *Ocean Engineering*, 51, 63–84. https://doi.org/10.1016/j.oceaneng.2012.05.001

[7] Xu, H., Hassani, V., Guedes Soares, C., 2020. Truncated Least Square Support Vector Machine for Parameter Estimation of a Nonlinear Manoeuvring Model Based on PMM Tests. *Applied Ocean Research*, 97, 102076. https://doi.org/10.1016/j.apor.2020.102076

[8] Sukas, O. F., Kinaci, O. K., Bal, S., 2021. Asymmetric Ship Maneuvering Due to Twisted Rudder Using System-Based and Direct CFD Approaches. *Applied Ocean Research*, 108, 102529. https://doi.org/10.1016/j.apor.2021.102529

[9] Dai, K., Li, Y., 2021. Experimental and Numerical Investigation on Maneuvering Performance of Small Waterplane Area Twin Hull. *Brodogradnja*, 72(2), 93–114. https://doi.org/10.21278/brod72206

[10] American Bureau of Shipping, 2017. Guide for Vessel Maneuverability, American Bureau of Shipping, Houston.

[11] Mikulec, M., Piehl, H., 2023. Verification and Validation of CFD Simulations with Full-Scale Ship Speed/Power Trial Data. *Brodogradnja*, 74, 41–62. https://doi.org/10.21278/brod74103

[12] Mei, B., Sun, L., Shi, G., 2020. Full-Scale Maneuvering Trials Correction and Motion Modelling Based on Actual Sea and Weather Conditions. *Sensors*, 20(14), 3963. https://doi.org/10.3390/s20143963

[13] Goodman, A., Gertler, M., Kohl, R., 1976. Experimental Techniques and Methods of Analysis Used at Hydronautics for Surface-Ship Maneuvering Predictions, *11th Naval Hydrodynamics Symposium* 28 March-2 April, London, England.

[14] Yasukawa, H., Yoshimura, Y., 2015. Introduction of MMG Standard Method for Ship Maneuvering Predictions. *Journal of Marine Science and Technology*, 20(1), 37–52. https://doi.org/10.1007/s00773-014-0293-y

[15] Permanent International Association of Navigation Congresses Permanent Technical Committee II, Working Group No. 20, 1992. Capability of Ship Manoeuvring Simulation Models for Approach Channels and Fairways in Harbours: Report of Working Group No. 20, *PIANC.*

[16] Kostoulas, C., 2017. Container Vessel Maneuvering Model in Shallow Waters and Assessment of Maneuvering Coefficients through System Identification. Master's Thesis, *KTH Royal Institute of Technology, School of Architecture and the Built Environment*.

[17] Araki, M., 2013. Ship Maneuvering Mathematical Model Using System Identification Technique with Experimental and CFD Free Running Trials in Calm Water and Astern Waves. PhD's Thesis, *Osaka University*.

[18] Zhang, G., Zhang, X., Pang, H., 2015. Multi-Innovation Auto-Constructed Least Squares Identification for 4 DOF Ship Manoeuvring Modelling with Full-Scale Trial Data. *ISA Transactions*, 58, 186–195. https://doi.org/10.1016/j.isatra.2015.04.004

[19] Källström, C., 1979. Identification and Adaptive Control Applied to Ship Steering. PhD's Thesis, *Lund Institute of Technology*.

[20] Ødegård, V., 2009. Nonlinear Identification of Ship Autopilot Models. Master's Thesis, *Norwegian University of Science and Technology*.

[21] Mauro, F., Kana, A. A., 2023. Digital Twin for Ship Life-Cycle: A Critical Systematic Review. *Ocean Engineering*, 269, 113479. https://doi.org/10.1016/j.oceaneng.2022.113479

[22] Han, Y., Hao, L., Shi, C., Pan, Z., Gu, M., 2023. Prediction of Ship Maneuvering Motion with Grey-Box Modelling Incorporating Mechanism and Data. *Ships and Offshore Structures*, 1–14. https://doi.org/10.1080/17445302.2023.2231207

[23] Xue, Y., Liu, Y., Ji, C., Xue, G., Huang, S., 2020. System Identification of Ship Dynamic Model Based on Gaussian Process Regression with Input Noise. *Ocean Engineering*, 216, 107862. https://doi.org/10.1016/j.oceaneng.2020.107862

[24] Jiang, L., Shang, X., Jin, B., Ji, C., Zhang, Z., 2024. Multi-Objective Optimal Input Design for Grey-Box Identification Modelling of Ship Manoeuvring Motion. *Ships and Offshore Structures*, 1–10. https://doi.org/10.1080/17445302.2024.2335452

[25] Nomoto, K., Taguchi, T., Honda, K., Hirano, S., 1957. On the Steering Qualities of Ships. *International Shipbuilding Progress*, 4(35), 354–370. https://doi.org/10.3233/ISP-1957-43504

[26] Abkowitz, M. A., 1964. Lectures on Ship Hydrodynamics. Steering and Manoeuvrability. *TU Delft Publication*, Report No: Hy-5, Hydro and Aerodynamics Laboratory, Lyngby, Denmark.

[27] Ogawa, A., Kasai, H., 1978. On the Mathematical Model of Manoeuvring Motion of Ships. *International Shipbuilding Progress*, 25(292), 306–319. https://doi.org/10.3233/ISP-1978-2529202

[28] Yoshimura, Y., 2005. Mathematical Model for Manoeuvring Ship Motion (MMG Model). *Workshop on Mathematical Models for Operations Involving Ship-Ship Interaction*, 4-5 August, Tokyo, Japan, 1–6.

[29] Milanov, E., 2014. Sea Vehicle Maneuvering Model Identification by 'Grey Box' Method. *Proceeding of 4th International Conference on Material Science, Hydro-and Aerodynamics and National Security*, 225–231.

[30] Efremov, D., Milanov, E., 2019. Identification of the Twin Propellers–Twin Rudder System in Vessel Simulation Model by 'Grey-Box' Method. *Sustainable Development and Innovations in Marine Technologies*, CRC Press, 175–181. https://doi.org/10.1201/9780367810085-22

[31] Liu, Y., Xue, Y., Huang, S., Jing, Q., Xue, G., 2020. Gray-and Black-Box Modeling of Ships and Wave Energy Converters Based on Bayesian Regression, *Preprints*, 2020090365. https://doi.org/10.20944/preprints202009.0365.v1

[32] Zhang, Z., Zhang, Y., Wang, J., Wang, H., 2022. Parameter Identification and Application of Ship Maneuvering Model Based on TO-CSA. *Ocean Engineering*, 266, 113128. https://doi.org/10.1016/j.oceaneng.2022.113128

[33] Alexandersson, M., Mao, W., Ringsberg, J. W., 2022. System Identification of Vessel Manoeuvring Models. *Ocean Engineering*, 266, 112940. https://doi.org/10.1016/j.oceaneng.2022.112940

[34] Chen, L., Yang, P., Li, S., Tian, Y., Liu, G., Hao, G., 2022. Grey-Box Identification Modeling of Ship Maneuvering Motion Based on LS-SVM. *Ocean Engineering*, 266, 112957. https://doi.org/10.1016/j.oceaneng.2022.112957

[35] Zhang, R., Zhang, X., Wang, X., 2022. Gray-Box Modeling of Ship Manoeuvring Motion Using On-Line Support Vector Machine. *4th International Conference on Applied Machine Learning (ICAML)*, 23-25 July, Changsha, China, 1–4. https://doi.org/10.1109/ICAML57167.2022.00051

[36] Chillcce, G., el Moctar, O., 2023. Data-Driven System Identification of Hydrodynamic Maneuvering Coefficients from Free-Running Tests. *Physics of Fluids*, 35(5). https://doi.org/10.1063/5.0148219

[37] Sutulo, S., Guedes Soares, C., 2023. Application of an Offline Identification Algorithm for Adjusting Parameters of a Modular Manoeuvring Mathematical Model. *Ocean Engineering*, 279, 114328. https://doi.org/10.1016/j.oceaneng.2023.114328

[38] Sukas, O. F., Kinaci, O. K., Bal, S., 2019. Theoretical Background and Application of MANSIM for Ship Maneuvering Simulations. *Ocean Engineering*, 192, 106239. https://doi.org/10.1016/j.oceaneng.2019.106239

[39] SIMMAN, 2008. Part C: Captive and Free Model Test Data.

[40] Yoshimura, Y., Masumoto, Y., 2011. Hydrodynamic Force Database with Medium High Speed Merchant Ships Including Fishing Vessels and Investigation into a Manoeuvring Prediction Method. *Journal of the Japan Society of Naval Architects and Ocean Engineers*, 14, 63–73. https://doi.org/10.2534/jjasnaoe.14.63

[41] Wu, G., Li, Y., Jiang, C., Wang, C., Guo, J., Cheng, R., 2022. Multi-Vessels Collision Avoidance Strategy for Autonomous Surface Vehicles Based on Genetic Algorithm in Congested Port Environment. *Brodogradnja*, 73(3), 69–91. https://doi.org/10.21278/brod73305

[42] Holtrop, J., Mennen, G. G. J., 1982. An Approximate Power Prediction Method. *International Shipbuilding Progress*, 29(335), 166–170. https://doi.org/10.3233/ISP-1982-2933501

[43] Holtrop, J., 1984. A Statistical Re-Analysis of Resistance and Propulsion Data. Published in *International Shipbuilding Progress*, ISP, 31(363).

[44] Xhaferaj, B., 2022. Investigation on Some Conventional Hulls Forms of the Predictive Accuracy of a Parametric Software for Preliminary Predictions of Resistance and Power. *Brodogradnja*, 73(1), 1–22. https://doi.org/10.21278/brod73101

[45] Pillonetto, G., Chen, T., Chiuso, A., De Nicolao, G., Ljung, L., 2022. Regularized System Identification: Learning Dynamic Models from Data, *Springer Nature*. https://doi.org/10.1007/978-3-030-95860-2

[46] Ljung, L., Andersson, C., Tiels, K., Schön, T. B., 2020. Deep Learning and System Identification. *IFAC-PapersOnLine*, 53(2), 1175–1181. https://doi.org/10.1016/j.ifacol.2020.12.1329

[47] Ljung, L., 1999. System Identification: Theory for the User, *Prentice Hall PTR.*

[48] Ljung, L., Singh, R., Chen, T., 2015. Regularization Features in the System Identification Toolbox. *IFAC-PapersOnLine*, 48(28), 745–750. https://doi.org/10.1016/j.ifacol.2015.12.219

[49] Ljung, L., 2012. System Identification Toolbox User's Guide (Release 2012b), *The MathWorks, Inc.*

[50] Coleman, T. F., Li, Y., 1996. An Interior Trust Region Approach for Nonlinear Minimization Subject to Bounds. *SIAM Journal of Optimization*, 6(2), 418–445. https://doi.org/10.1137/0806023

[51] Zhang, J., Zhang, Y., 2021. A Novel Ship-Ship Distance Model in Restricted Channel via Gaussian-TRR Identification. *Mathematical Problems in Engineering*, 2021, 1–19. https://doi.org/10.1155/2021/6626850

[52] Gao, X., Hou, Q., Yao, S., Zhou, K., 2023. Opposite Normalized Trust-Region Reflective (ONTRR): A New Algorithm for Parameter Extraction of Single, Double and Triple Diode Solar Cell Models. *Applied Sciences*, 13(14), 8199. https://doi.org/10.3390/app13148199

[53] Yoshimura, Y., 1986. Mathematical Model for the Manoeuvring Ship Motion in Shallow Water. *Journal of the Kansai Society of Naval Architects*, (No.200).

[54] Taimuri, G., Matusiak, J., Mikkola, T., Kujala, P., Hirdaris, S., 2020. A 6-DoF Maneuvering Model for the Rapid Estimation of Hydrodynamic Actions in Deep and Shallow Waters. *Ocean Engineering*, 218, 108103. https://doi.org/10.1016/j.oceaneng.2020.108103

[55] Ljung, L., Singh, R., Zhang, Q., Lindskog, P., Iouditski, A., 2009. Developments in The MathWorks System Identification Toolbox. *IFAC Proceedings Volumes*, 42(10), 522–527. https://doi.org/10.3182/20090706-3-FR-2004.00086

[56] Fossen, T. I., 2002. Marine Control Systems: Guidance, Navigation, and Control of Ships, Rigs and Underwater Vehicles. *Marine Cybernetics,* Trondheim, NORWAY.

[57] Perez, T., and Blanke, M.,2002. Mathematical Ship Modeling for Control Applications. *Technical University of Denmark.*

[58] Perez, T., Smogeli, O., Fossen, T., Sorensen, A. J., 2006. An Overview of the Marine Systems Simulator (MSS): A Simulink Toolbox for Marine Control Systems. *Modeling, Identification and Control*, 27(4), 259–275. https://doi.org/10.4173/mic.2006.4.4

[59] Xue, D., Chen, Y., 2013. System Simulation Techniques with MATLAB and Simulink. *John Wiley & Sons,* West Sussex.

[60] Sutulo, S., Guedes Soares, C., 2021. Review on Ship Manoeuvrability Criteria and Standards. *Journal of Marine Science and Engineering*, 9(8), 904. https://doi.org/10.3390/jmse9080904

[61] IMO, 2002. Annex 6 Standards for Ship Manouverability. *IMO Resolution MSC.137(76)*.

[62] Kinaci, O. K., Ozturk, D., 2022. Straight-Ahead Self-Propulsion and Turning Maneuvers of DTC Container Ship with Direct CFD Simulations. *Ocean Engineering*, 244, 110381. https://doi.org/10.1016/j.oceaneng.2021.110381

[63] Bose, B. P., Dhar, M., 2022. Dredged Sediments Are One of the Valuable Resources: A Review. *International Journal of Earth Sciences Knowledge and Applications*, 4(2), 324–331.

Appendix 1: Extended results

A.1 Parameter identification for car carrier and KVLCC2

Table A.1 Estimated non-dimensional hydrodynamic hull coefficients of the 3-DOF model by empirical method and SI method for car carrier, initial

i	Parameter	Empirical	Identified version			
			Adjustment interval	TRR	Adaptive Gauss-Newton line search (Wills-Ninness)	Gradient-descent line search
		θ_{0i} for 200	b_i	θ_i for IV 201	θ_i for IV 202	θ_i for IV 203
1	X'_0	-0.0229	[-0.024, -0.020]	-0.0240	-0.0240	-0.0206
2	X'_{vv}	-0.0400	[-0.50, 0.00]	-0.0001	-0.0141	-0.0497
3	X'_{vr}	0.0212	[0.00, 1.00]	0.1230	0.0121	0.0407
4	X'_{rr}	0.0001	[0.00, 1.00]	0.0002	0.0000	0.0110
5	X'_{vvvv}	0.2869	[0.00, 1.00]	0.9960	0.3006	0.2866
6	Y'_v	-0.3267	[-3.00, -0.30]	-0.3012	-1.0710	-0.3171
7	Y'_r	0.0781	[0.00, 0.30]	0.0630	0.0000	0.0648
8	Y'_{vvv}	-1.5986	[-7.00, -1.20]	-5.5359	-1.6597	-1.5985
9	Y'_{vvr}	-0.7500	[-8.00, 0.00]	-0.6896	-0.6932	-0.7500
10	Y'_{vrr}	-0.5250	[-4.00, 0.00]	-0.5880	-0.5811	-0.5253
11	Y'_{rrr}	-0.0510	[-0.30, 0.00]	-0.0026	-0.1637	-0.0496
12	N'_v	-0.0995	[-0.50, 0.00]	-0.1938	-0.2813	-0.2027
13	N'_r	-0.0418	[-0.20, 0.00]	-0.0157	-0.0200	-0.0253
14	N'_{vvv}	-0.1522	[-1.00, 0.00]	-0.0002	-0.3658	-0.1555
15	N'_{vvr}	-0.5713	[-2.00, 0.00]	-1.1196	-0.3804	-0.5655
16	N'_{vrr}	0.0217	[-0.09, 1.00]	-0.0900	0.0747	0.0132
17	N'_{rrr}	-0.0256	[-0.30, 0.00]	-0.0379	-0.0291	-0.0334
18	l'_r	-0.9931	[-1.50, -0.70]	-0.84164	-0.9772	-0.9883
19	ε	1.0188	[1.00, 1.70]	1.00248	1.0089	1.0299
20	m'_x	0.0122	[0.01, 0.10]	0.01004	0.0200	0.0100
21	m'_y	0.1737	[0.01, 0.40]	0.35399	0.3930	0.1993
22	J'_z	0.0099	[0.0095, 0.0195]	0.00950	0.0095	0.0142
23	t_R	0.3900	[0.15, 0.40]	0.39789	0.2897	0.3875
24	a_H	0.4382	[0.30, 0.50]	0.34875	0.3027	0.4383
25	x'_H	-0.4000	[-0.50, -0.30]	-0.49977	-0.4692	-0.4014
26	t_P	0.2700	[0.10, 0.40]	0.14168	0.1305	0.2898
27	w_{P0}	0.3180	[0.15, 0.55]	0.29650	0.2958	0.3074
28	$\gamma_{R_{upper}}$	0.5266	[0.50, 0.90]	0.52711	0.5987	0.5266
29	$\gamma_{R_{lower}}$	0.3948	[0.40, 0.70]	0.42763	0.5984	0.4010

Table A.1 (continued)

i	Parameter	Identified version		
		Adjustment interval	SQP	Levenberg-Marquardt
		b_i	θ_i for IV 204	θ_i for IV 205
1	X'_0	[-0.024, -0.020]	-0.0237	-0.0240
2	X'_{vv}	[-0.50, 0.00]	-0.0413	-0.0030
3	X'_{vr}	[0.00, 1.00]	0.0239	0.0139
4	X'_{rr}	[0.00, 1.00]	0.0000	0.0000
5	X'_{vvvv}	[0.00, 1.00]	0.2868	0.2668
6	Y'_v	[-3.00, -0.30]	-0.3255	-0.7622
7	Y'_r	[0.00, 0.30]	0.0758	0.0083
8	Y'_{vvv}	[-7.00, -1.20]	-1.5986	-1.4709
9	Y'_{vvr}	[-8.00, 0.00]	-0.7501	-0.9909
10	Y'_{vrr}	[-4.00, 0.00]	-0.5249	-0.2901
11	Y'_{rrr}	[-0.30, 0.00]	-0.0514	0.0000
12	N'_v	[-0.50, 0.00]	-0.1115	-0.1701
13	N'_r	[-0.20, 0.00]	-0.0173	0.0000
14	N'_{vvv}	[-1.00, 0.00]	-0.1526	-0.3362
15	N'_{vvr}	[-2.00, 0.00]	-0.5704	-0.0370
16	N'_{vrr}	[-0.09, 1.00]	0.0198	-0.0485
17	N'_{rrr}	[-0.30, 0.00]	-0.0215	-0.0675
18	l'_r	[-1.50, -0.70]	-0.9924	-1.1550
19	ε	[1.00, 1.70]	1.0203	1.0000
20	m'_x	[0.01, 0.10]	0.0113	0.0628
21	m'_y	[0.01, 0.40]	0.1766	0.4000
22	J'_z	[0.0095, 0.0195]	0.0184	0.0095
23	t_R	[0.15, 0.40]	0.3896	0.4000
24	a_H	[0.30, 0.50]	0.4382	0.4377
25	x'_H	[-0.50, -0.30]	-0.4001	-0.4997
26	t_P	[0.10, 0.40]	0.2728	0.1094
27	w_{P0}	[0.15, 0.55]	0.3166	0.5500
28	$\gamma_{R_{upper}}$	[0.50, 0.90]	0.5266	0.6857
29	$\gamma_{R_{lower}}$	[0.40, 0.70]	0.3940	0.6600

Table A.1 summarize the hydrodynamic coefficients and parameters obtained from a range of identified models for car carrier. In Tables A.1 A.2, and A.3, b_i is adjustment interval with a lower bound (LB) and an upper bound (UB). Propeller and rudder parameters of 3-DOF MMG model were kept fixed for KVLCC2. The following fixed parameter values were used: l'_r, ε, m'_x, m'_y, J'_z, t_R, a_H, x'_H, t_P, w_{P0}, $\gamma_{R_{upper}}$, $\gamma_{R_{lower}}$ as 0.710, 1.09, 0.022, 0.223, 0.011, 0.387, 0.312, -0.464, -0.500, 0.220, 0.350, 0.640 and 0.395, respectively, from the study of Sukas et al. [38]. The hydrodynamic hull coefficients of KVLCC2 listed in Table A.2 were

free for identification. Therefore, estimates of hull coefficients were investigated. The initial hull coefficients of the 3-DOF MMG model, and its boundaries, estimated by SI, are presented in Table A.2.

Table A.2 Estimated non-dimensional hydrodynamic hull coefficients of the 3-DOF model from the SI method for KVLCC2

i	Parameter	MANSIM [38]	Identified version			
			TRR	TRR		TRR
		θ_{0i} for IV 100	θ_i for IV 101	θ_i for IV 102	b_i for IV 103	θ_i for IV 103
1	X'_0	-0.02200	-0.0219	-0.0219	[-0.23, -0.21]	-0.0219
2	X'_{vv}	-0.04000	0.1867	0.1864	[-1.00, 0.00]	-0.0016
3	X'_{vr}	0.00200	-0.0157	-0.0157	[0.00, 1.00]	0.0053
4	X'_{rr}	0.01100	0.0083	0.0083	[0.00, 1.00]	0.0204
5	X'_{vvvv}	0.77100	-0.2574	-0.2605	[0.00, 1.00]	0.9892
6	Y'_v	-0.31500	-0.3925	-0.3922	[-1.00, 0.00]	-0.3276
7	Y'_r	0.08300	0.1028	0.1029	[0.00, 1.00]	0.0977
8	Y'_{vvv}	-1.60700	-0.1726	-0.2084	[-2.00, 0.00]	-1.6326
9	Y'_{vvr}	0.37900	-0.3813	-0.4225	[0.00, 1.00]	0.3953
10	Y'_{vrr}	-0.39100	-1.0571	-1.0733	[-1.00, 0.00]	-0.3529
11	Y'_{rrr}	0.00800	-0.1438	-0.1460	[0.00, 1.00]	0.0000
12	N'_v	-0.13700	-0.1392	-0.1391	[-1.00, 0.00]	-0.1370
13	N'_r	-0.04900	-0.0356	-0.0356	[-1.00, 0.00]	-0.0458
14	N'_{vvv}	-0.03000	-1.2394	-1.2506	[-1.00, 0.00]	-0.0272
15	N'_{vvr}	-0.29400	-2.0769	-2.0898	[-1.00, 0.00]	-0.3157
16	N'_{vrr}	0.05500	-0.7587	-0.7635	[0.00, 1.00]	0.0460
17	N'_{rrr}	-0.01300	-0.1267	-0.1273	[-1.00, 0.00]	-0.0078

Table A.3 summarize the hydrodynamic coefficients and parameters obtained from a range of identified models combined with varied line search method for car carrier.

Table A.3 Estimated non-dimensional hydrodynamic hull coefficients of the 3-DOF model by empirical method and SI method for car carrier, final

i	Parameter	Identified version			
		Adjustment interval	TRR	TRR with Regularization	Adaptive Gauss-Newton line search (Wills-Ninness)
		b_i	θ_i for IV 201	θ_i for IV 211	θ_i for IV 212
1	X'_0	[-0.024, -0.020]	-0.0240	-0.0240	-0.0240
2	X'_{vv}	[-0.50, 0.00]	-0.0001	-0.0014	-0.0006
3	X'_{vr}	[0.00, 1.00]	0.1230	0.1156	0.1083
4	X'_{rr}	[0.00, 1.00]	0.0002	0.0002	0.0000
5	X'_{vvvv}	[0.00, 1.00]	0.9960	0.6073	0.7099
6	Y'_v	[-3.00, -0.30]	-0.3012	-0.3018	-0.3147
7	Y'_r	[0.00, 0.30]	0.0630	0.0754	0.0651
8	Y'_{vvv}	[-7.00, -1.20]	-5.5359	-1.9029	-2.1093
9	Y'_{vvr}	[-8.00, 0.00]	-0.6896	-0.3653	-0.3496
10	Y'_{vrr}	[-4.00, 0.00]	-0.5880	-0.7378	-0.7032
11	Y'_{rrr}	[-0.30, 0.00]	-0.0026	-0.0326	-0.0188
12	N'_v	[-0.50, 0.00]	-0.1938	-0.1657	-0.1928
13	N'_r	[-0.20, 0.00]	-0.0157	-0.0105	-0.0206
14	N'_{vvv}	[-1.00, 0.00]	-0.0002	-0.1207	-0.1299
15	N'_{vvr}	[-2.00, 0.00]	-1.1196	-0.8705	-0.7873
16	N'_{vrr}	[-0.09, 1.00]	-0.0900	0.0595	0.0383
17	N'_{rrr}	[-0.30, 0.00]	-0.0379	-0.0120	-0.0062
18	l'_r	[-1.50, -0.70]	-0.84164	-0.8946	-0.9526
19	ε	[1.00, 1.70]	1.00248	1.0022	1.0013
20	m'_x	[0.01, 0.10]	0.01004	0.0103	0.0100
21	m'_y	[0.01, 0.40]	0.35399	0.2835	0.2899
22	J'_z	[0.0095, 0.0195]	0.00950	0.0129	0.0097
23	t_R	[0.15, 0.40]	0.39789	0.3902	0.4000
24	a_H	[0.30, 0.50]	0.34875	0.4029	0.4072
25	x'_H	[-0.50, -0.30]	-0.49977	-0.4018	-0.4580
26	t_P	[0.10, 0.40]	0.14168	0.2079	0.1822
27	w_{P0}	[0.15, 0.55]	0.29650	0.3564	0.3559
28	$\gamma_{R_{upper}}$	[0.50, 0.90]	0.52711	0.5266	0.5399
29	$\gamma_{R_{lower}}$	[0.40, 0.70]	0.42763	0.4186	0.4449

Table A.3 (continued)

i	Parameter	Adjustment interval	Identified version TRR with Gradient-descent line	TRR with SQP	TRR with Levenberg-Marquardt
		b_i	θ_i for IV 213	θ_i for IV 214	θ_i for IV 215
1	X'_0	[-0.024, -0.020]	-0.0240	-0.0240	-0.0240
2	X'_{vv}	[-0.50, 0.00]	-0.0007	-0.0018	0.0000
3	X'_{vr}	[0.00, 1.00]	0.1154	0.1153	0.1096
4	X'_{rr}	[0.00, 1.00]	0.0000	0.0004	0.0000
5	X'_{vvvv}	[0.00, 1.00]	0.7100	0.7099	0.7101
6	Y'_v	[-3.00, -0.30]	-0.3000	-0.3022	-0.3006
7	Y'_r	[0.00, 0.30]	0.0830	0.0758	0.0692
8	Y'_{vvv}	[-7.00, -1.20]	-2.1107	-2.1105	-2.1109
9	Y'_{vvr}	[-8.00, 0.00]	-0.3456	-0.3466	-0.3453
10	Y'_{vrr}	[-4.00, 0.00]	-0.7112	-0.7071	-0.7119
11	Y'_{rrr}	[-0.30, 0.00]	-0.0186	-0.0352	-0.0178
12	N'_v	[-0.50, 0.00]	-0.2009	-0.2019	-0.1952
13	N'_r	[-0.20, 0.00]	-0.0243	-0.0173	-0.0222
14	N'_{vvv}	[-1.00, 0.00]	-0.1318	-0.1312	-0.1315
15	N'_{vvr}	[-2.00, 0.00]	-0.7895	-0.7924	-0.7899
16	N'_{vrr}	[-0.09, 1.00]	0.0528	0.0639	0.0552
17	N'_{rrr}	[-0.30, 0.00]	-0.0001	-0.0157	-0.0012
18	l'_r	[-1.50, -0.70]	-0.9429	-0.9417	-0.9431
19	ε	[1.00, 1.70]	1.0003	1.0061	1.0000
20	m'_x	[0.01, 0.10]	0.0105	0.0104	0.0100
21	m'_y	[0.01, 0.40]	0.2895	0.2747	0.2866
22	J'_z	[0.0095, 0.0195]	0.0095	0.0127	0.0101
23	t_R	[0.15, 0.40]	0.3880	0.3864	0.3897
24	a_H	[0.30, 0.50]	0.4084	0.4114	0.4062
25	x'_H	[-0.50, -0.30]	-0.4556	-0.4533	-0.4557
26	t_P	[0.10, 0.40]	0.1960	0.2074	0.1910
27	w_{P0}	[0.15, 0.55]	0.3525	0.3487	0.3559
28	$\gamma_{R_{upper}}$	[0.50, 0.90]	0.5279	0.5268	0.5286
29	$\gamma_{R_{lower}}$	[0.40, 0.70]	0.4334	0.4322	0.4374

A.2 Prediction errors for car carrier and KVLCC2

The prediction errors obtained from the identified models used for KVLCC2 were analysed. Table A.4 shows that the IV 101 and IV 102 models are more appropriate than the IV 103 model based on Akaike's information criterion. However, Fig. 6 suggests that IV 103 model was found to be better in predicting the heading angle of KVLCC2.

Table A.4 Identified model selection scores (AICc, BIC, and FPE) on training data of Manoeuvre No. 1.a with varying bounds for KVLCC2

IV #	AICc	BIC	FPE
101	-1.5521E+05	-1.5509E+05	1.3424E-18
102	-1.5521E+05	-1.5509E+05	1.3426E-18
103	-1.3237E+05	-1.3225E+05	2.1957E-16

It can be seen that there are no significant differences between the IV 101 and IV 102 models of KVLCC2, only yaw NRMSE value is different, as shown in Table A.5.

Table A.5 MSE and NRMSE of ship motion (Surge and sway velocity as well as yaw rate) prediction responses on training data of Manoeuvre No. 1.a with varying search method with bounds for KVLCC2

IV #	MSE	Surge velocity *u* [-] NRMSE	Sway velocity *v* [-] NRMSE	Yaw rate *r* [-] NRMSE
101	0.0000	0.0009	0.0020	0.2287
102	0.0000	0.0009	0.0020	0.2285
103	0.0001	0.0092	0.0074	0.0841

The prediction errors obtained from various identified models for the car carrier are presented in Tables A.6 and A.7. Despite the model with the lowest value of AICc and BIC indicating that model IV 212 was the optimal choice among the alternatives, model IV 215 demonstrated a very close match to the free manoeuvring data of Manoeuvre 1.b. This is in line with the results of the NRMSE value for the yaw rate for model IV 215.

Table A.6 MSE and NRMSE of ship motion (Surge and sway velocity as well as yaw rate) prediction responses on training data of Manoeuvre No. 1.b with varying search methods with bounds for the car carrier

IV #	MSE	Surge velocity *u* [-] NRMSE	Sway velocity *v* [-] NRMSE	Yaw rate *r* [-] NRMSE
201	0.0009	0.1015	0.2403	0.0820
202	0.0015	0.1440	0.2696	0.1510
203	0.0030	0.1927	0.4396	0.1043
204	0.0052	0.2463	0.5462	0.2428
205	0.0078	0.5067	0.2788	0.1066
211	0.0011	0.1114	0.2607	0.0753
212	0.0012	0.0908	0.2930	0.0825
213	0.0012	0.0869	0.3092	0.0920
214	0.0011	0.1133	0.2656	0.0745
215	0.0011	0.1041	0.2807	0.0695

Table A.7 Identified model selection scores (AICc, BIC, and FPE) on training data of Manoeuvre No. 1.b with varying search methods with bounds for the car carrier

IV #	AICc	BIC	FPE
201	-8.2599E+03	-8.1308E+03	9.0569E-12
202	-7.2109E+03	-7.0819E+03	9.9879E-11
203	-7.1160E+03	-6.9814E+03	1.2570E-10
204	-5.8786E+03	-5.7496E+03	2.1063E-09
205	-6.5036E+03	-6.3746E+03	5.0395E-10
211	-8.1399E+03	-8.1025E+03	1.1919E-11
212	-8.3901E+03	-8.2610E+03	6.7244E-12
213	-8.3168E+03	-8.1877E+03	7.9516E-12
214	-8.1172E+03	-7.9881E+03	1.2556E-11
215	-8.3361E+03	-8.2070E+03	7.6080E-12

A.3 Comparison of identified models with regularization option for car carrier

Velocity components were estimated utilising TRR models with regularisation options created with candidate λ and R values, which were then tested and compared with validation data as shown in Fig. A1.

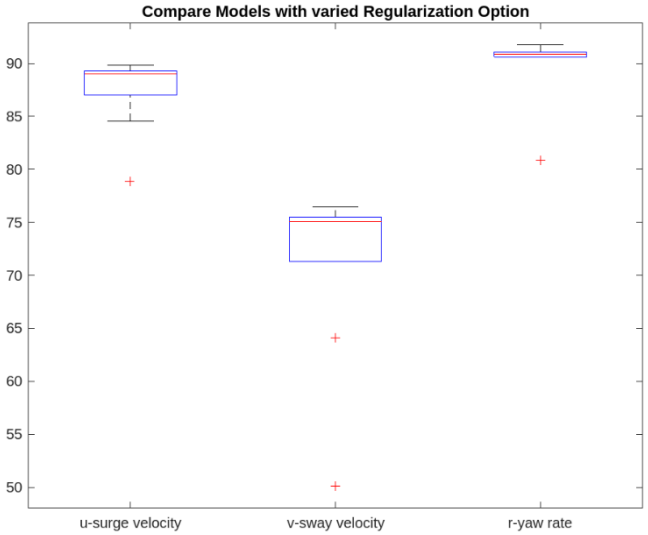

Fig. A1 Boxplot of the fits for Manoeuvre 1.b of car carrier